Title	Conformation and Dynamics of the Cellulose Chain in Ionic Liquids
Author(s)	前田, 綾香
Citation	大阪大学, 2014, 博士論文
Version Type	VoR
URL	https://doi.org/10.18910/34039
rights	
Note	

Conformation and Dynamics of the Cellulose Chain in Ionic Liquids

A Doctoral Thesis

by

Ayaka Maeda

Submitted to
the Graduate School of Science, Osaka University

February, 2014

Acknowledgements

This thesis work was carried out from 2011 to 2014 under the direction of Professors Takahiro Sato and Tadashi Inoue at the Department of Macromolecular Science, Graduate School of Science, Osaka University. The author wishes to express her sincerest gratitude to Professors Takahiro Sato and Tadashi Inoue for their kindest guidance, valuable suggestions and discussions during this work. The author also would like to extend her gratitude to associate Professors Akihito Hashidzume, Ken Terao, and Osamu Urakawa for their helpful advice and valuable discussions.

The author would like to express her deep gratitude to Professor Katsumi Imada at the Department of Macromolecular Science, Graduate School of Science, Osaka University for his careful review and valuable comments.

The author would like to gratefully acknowledge Professor Toshiyuki Shikata (the Institute for Chemical Technology, Division of Ecosciences, Tokyo University of Agriculture and Technology), Professor Masayuki Yamaguchi (Japan Advanced Institute of Science and Technology), Professor Hiroyuki Yano (Research Institute for Sustainable Humanosphere, Kyoto University), and Professor Tetsuo Kondo (Faculty of Agriculture, Kyushu University) for their kind provision of cellulose and pullulan samples and valuable comments.

The author appreciates the financial support by Grant-in-Aid for Research Fellows of the Japan Society for the Promotion of Science (12J01200).

The author thanks all members of both Sato and Inoue laboratories for their friendships.

Last but not least, the author expresses her sincerest thanks to her family and friends, for their constant support and warmest encouragements.

February, 2014
at Osaka

前田 綾香
Ayaka Maeda

Contents

Chapter I. General Introduction

Chapter II. Light Scattering Study on Cellulose in Ionic Liquids

Chapter V. Comparison between Cellulose and Other Polysaccharides

Chapter I. General Introduction

I-1. Polymer Chain Models

The main chain of a linear polymer molecule consists of many chemical bonds. Its structure can be specified in terms of the bond length b, bond angle θ, and internal rotation angle ϕ of each chemical bond. For most of polymer molecules, b and θ are approximately constant, but ϕ can change under the internal rotation potential $E(\phi)$. Due to the degree of freedom with respect to ϕ, polymer molecules can take a huge number of rotational isomeric states.

The number of the rotational isomeric states is too many to consider all states individually at the discussion on the polymer chain conformation. Thus, a coarse graining of the polymer molecule is necessary. The wormlike chain model is often used to discuss the thermally equilibrium conformation of the polymer chain and static properties of polymer solutions and melts. This coarse-grained model is specified by the persistence length q and the contour length L, or equivalently the Kuhn segment size $b_\mathrm{K} = 2q$ and the number of the Kuhn segments per chain $N_\mathrm{K} = L/2q$. The persistence length q (or b_K) is a parameter characterizing the *static rigidity* of the polymer chain, and the polymer chain with small and large q is referred to as the flexible and stiff polymers, respectively. When N_K is large enough, the wormlike chain is reduced to the Gauss chain. Therefore, for stiff polymers, the Gaussian statistics is expected only at very long L or high molecular weight.

The standard coarse-grained model used to discuss the polymer chain dynamics and dynamical properties of polymer solutions and melts is the Rouse model, which is a sequence of elastic springs connected by beads. Each spring is called the Rouse segment. The Rouse chain is characterized in terms of the Rouse segment size b_R and the number of the Rouse segments per chain N_R. The Rouse segment size b_R characterizes the *dynamic rigidity* of the polymer chain. The Rouse chain obeys the Gaussian statistics. If a sufficiently long linear polymer chain is viewed as a Gauss chain and also as a Rouse chain, and the relation of $b_K^2 N_K = b_R^2 N_R$ is obtained. However, the direct relation between b_K and b_R is not self-evident.

I-2. Static vs. Dynamic Polymer Chain Rigidities

The Kuhn segment size b_K or the persistence length q can be experimentally determined from the molecular weight dependence of the radius of gyration, the hydrodynamic radius, or the intrinsic viscosity. On the other hand, the Rouse segment size b_R is determined from the limiting modulus of the rubbery component at high frequencies.

Inoue and Osaki demonstrated that the Kuhn and Rouse segment sizes are almost identical for flexible polymers in melt. On the other hand, the Rouse segment size b_R for polystyrene, a typical flexible polymer, is more than five times larger than b_K in dilute solution. This indicates that b_R for polystyrene depends on the polymer concentration, because b_K is known to be independent of the concentration.

So far, polymer chain dynamics has been studied mostly on flexible polymers, and little has been known about the dynamic chain rigidity of stiff polymers. I was interested in the relation between the static and dynamic chain rigidities for the stiff polymer, and this thesis work was commenced. Among stiff polymers, cellulose was selected for the thesis work.

I-3. Previous Studies on Cellulose

I-3-1. Conformation of the Cellulose Chain

Cellulose consists of a long sequence of anhydroglucose residues, in which the glucose units are present in β-glucopyranose form, the 1−4′ positioned carbon atoms being linked through an ether bridge. The major part of native cellulose exists in the crystalline state. The spatial structure of the cellulose molecule in the crystalline state has been determined mainly by use of X-ray analysis. As described below, the obtained crystalline structure provides essential information about the conformation of the cellulose chain in solution, although the internal rotation angle about the glycoside bridge more or less fluctuates in solution.

As depicted in Figure I-1, the cellulosic chain has two kinds of internal rotational angles ϕ and ψ about two chemical bonds of the glucosidic bridges C(1)–O(1) and O(1)–C(4'). From crystallographic data for cellobiose (the dimer model of the cellulosic chain),$^{1)}$ the virtual bond length b is estimated to be 0.547 nm.

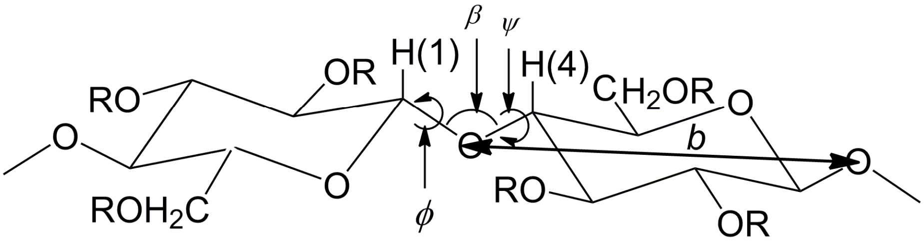

Figure I-1. Chemical structure of cellulose. The torsional angles ϕ and ψ are defined as the dihedral angles formed by the atoms H(1)C(1)O(1)C(4') and C(1)O(1)C(4')H(4'), respectively, measured relative to the cis conformation and being positive at the clockwise rotation along the vectors C(1)O(1) and O(1)C(4'), respectively.

Goebel, Harvie, and Brant$^{2)}$ calculated the internal rotation potential $E(\phi, \psi)$ for cellobiose. When the bond angle β of the glucosidic bridge in Figure I-1 is chosen to be 116° (the value for cellobiose in the crystalline state), $E(\phi, \psi)$ takes two energy minima at rotational states which correspond to a left-handed nearly 3/1 helical ($\phi = 50°$, $\psi = 0°$) and a nearly 2/1 helical or the zig-zag ($\phi = 22°$, $\psi = -35°$) state for the cellulosic chain taking repeatedly each rotational state (cf. Figure 3 in ref. 2). The two states give similar pitches h per the glucose residue, being 0.511 nm and 0.518 nm, respectively, and the energy barrier between the two states is not so high (< 2 kcal/mol).

Using $E(\phi, \psi)$ obtained and the geometry of the glucose residue taking the C1 chair conformation, Goebel et al. calculated the characteristic ratio C_∞ to be 103 at 25 °C. For the wormlike chain model, C_∞ is related to the persistence length q by[3,4)]

$$q = \left(b^2/2h\right)C_\infty \tag{I-1}$$

Thus, Goebel et al.'s result of C_∞ corresponds to q = 29.8 nm for the cellulose chain. This theoretical q value is considerably larger than experimental results for cellulose and its derivatives in literature. The disagreement between the theory and experiment in C_∞ has been already mentioned by Goebel et al. themselves.

Goebel et al. pointed out that if β is slightly increased from 116° to 125°, new energy minima appear in $E(\phi, \psi)$ in quite different rotational states, i.e., at $(\phi, \psi) \approx (0°, 180°)$ or $(180°, 0°)$ (cf. Figure 4 in ref. 2). When the cellulosic chain takes these new rotational states, the direction of the virtual bond abruptly changes along the chain. That is, kinks may occasionally appear on the cellulosic chain along with the bond angle fluctuation, and the chain may be viewed as a broken wormlike chain.[5)]

The *effective* persistence length for the broken wormlike chain can be written in the form[3-6)]

$$\frac{1}{q} = \frac{1}{q_0} + \frac{1-\cos\tilde{\theta}_\mathrm{K}}{h\exp\left(G^*/RT\right)} \tag{I-2}$$

where q_0 is the persistence length for the chain without the kink, $\tilde{\theta}_K$ is the kink angle, G^* is the excess free energy (per mole of the repeating unit) when the chain takes the kink conformation, and RT is the gas constant multiplied by the absolute temperature. As mentioned by Mansfield,[5)] the intrinsic viscosity for the normal wormlike and broken wormlike chains are indistinguishable if the parameter $\delta \equiv q(1 - \cos\ \tilde{\theta}_K)^2/2h\exp(G^*/RT)$ is sufficiently smaller than unity.

Yanai and Sato[6)] demonstrated good agreements of q and its temperature dependence for cellulose tris(phenylcarbamate) (CTC) in THF with theoretical results calculated by eq I-2 using q_0 of Goebel et al. mentioned above along with $\tilde{\theta}_K = 40°$ and $G^* = 4.9$ kJ/mol. The value of δ is less than 0.08, so that the broken wormlike chain model is indistinguishable from the wormlike chain model. The kink angle $\tilde{\theta}_K = 40°$ is realized by introducing in the 3/1 or 2/1 helical sequence a kink conformation $(\phi, \psi) \approx (170°, 0°)$,[4)] which is consistent with Goebel et al.'s $E(\phi, \psi)$ at $\beta = 125°$ (cf. Figure 4 in ref. 2). The value of G^* indicates that the kink appears in the cellulosic chain every seven glucose residues on average at 25 °C.

Goebel et al.[7)] also calculated the internal potential $E(\tilde{\phi}_1, \tilde{\phi}_3)$ for the amylosic chain. The result has a single shallow minimum at $(\tilde{\phi}_1, \tilde{\phi}_3) = (-19, -44)$ corresponding to a left-handed 5/1 helix, which forms a contrast to a rather deep double-well type potential for the cellulosic, in spite of the resemblance in the chemical structure between the two polysaccharides. Brant and Dimpfl[8)] further estimated the characteristic ratio C_∞ of amylose to be 5.5 from $E(\tilde{\phi}_1, \tilde{\phi}_3)$, and the result was favorably compared with experimental data.[9)] The standard deviation of the torsional fluctuation for $\tilde{\phi}_1$ and $\tilde{\phi}_3$ for amylose can be calculated from this C_∞ in a similar way to cellulose. The geometrical parameters of the amylosic chain can be extracted from the crystallographic data for methyl β-D-maltopyranoside.[10)] The result is much larger than that of cellulose due to the shallowness of $E(\tilde{\phi}_1, \tilde{\phi}_3)$. Although the helical nature of the amylosic chain was pointed out by several authors,[9,11-13] the global conformation of amylose may be regarded as the random coil due to this large torsional fluctuation.

I-3-2. Solvents for Cellulose

Cellulose is insoluble in common simple solvents. This poor solubility coming from hydrogen bonds of OH groups makes it difficult to characterize the conformation of the cellulose chain, though cellulose is one of the oldest macromolecules studied. The first report on the solvent for cellulose was made by Schweizer, who discovered a solution of cupric hydroxide in aqueous ammonia (cuoxam) dissolve cellulose strongly 14). After this report, several kinds of aqueous solutions containing metal complex were found to dissolve cellulose. However, most of aqueous metal complexes are not useful, because they are unstable, colored, highly toxic, or cause degradation of cellulose.

Industrially, *N*-methylmorpholine-*N*-oxide (NMMO) has become a desirable solvent for producing cellulose fiber. NMMO, however, is limited in use at the laboratory because of high cost and harsh condition required for dissolution of cellulose. In addition, McCormick *et al.* has stated that a solution of Lithium chloride (LiCl) in *N*,*N*-Dimethylacetamide (DMAc) is desirable solvent for cellulose because no degradation of cellulose occur in this solvent15).

I-3-3. Light Scattering Studies on Cellulose Solutions

By use of the above solvents (metal complex aqueous solution, NMMO, and LiCl/DMAc), light scattering measurements for cellulose solutions have been carried out so far. Light scattering is a powerful method to elucidate the polymer conformation. Most of light scattering measurements on cellulose solutions were made by using aqueous metal complexes owing to their strong dissolution ability[16-18]. According to these measurements, the persistence length *q* reflecting the static chain rigidity was around 4 nm for cellulose. On the other hand, McCormick reported *q* of cellulose to be 25.2 nm utilizing LiCl/DMAc as a solvent[15]. This value is much higher than those in aqueous metal complexes, and close to that theoretically predicted by Goebel et al. mentioned above. Moreover, Yanagisawa et al. reported *q* of cellulose in LiCl/DMAc to be 9 nm using the SEC-MALS-QELS (size-exclusion chromatography equipped with multi-angle light scattering and quasi-elastic light scattering detectors) method[19]. The reason for the difference in *q* between the two research groups has not been cleared. One may point out following problems about LiCl/DMAc: the gelation of cellulose in solution, incomplete dissolution of cellulose, and degradation of cellulose by heating during the dissolution process. These results suggest that *q* depends on the solvent species and measurement conditions. In order to clarify the chain stiffness of cellulose, more data should be accumulated to discuss the solvent dependence of the cellulose chain rigidity.

I-3-4. Ionic Liquids as a New Solvent for Cellulose

As mentioned above, useful solvents of cellulose are little available. In 2002, Rogers et al[20] reported that an ionic liquid, 1-buthyl-3-methylimidazolium chloride (BmimCl), can dissolve cellulose up to high concentrations. Ionic liquids are considered as preferred solvents in green and sustainable chemistry because of many advantages such as safety, extremely low volatility, and ease of recycling properties, in comparison with ordinary solvents. Ionic liquids become to play a more important role in industry as the polymer processing reagent.

Since Rogers et al.'s report, the system of cellulose and ionic liquid has attracted much attention of academic researchers, and its solution properties and dissolution mechanism have been studied extensively[21-24]. Remsing et al. revealed that the chloride ion (Cl^-) works as an accepter of proton in hydroxyl group of cellulose very effectively, which breaks intermolecular hydrogen bonds to dissolve cellulose[21)]. Hence, ionic liquids containing Cl^- as the anion have the ability of cellulose dissolution. However, it is rather difficult to apply light or X-ray scattering methods to these solvent systems because of high viscosity and strong absorption of X-ray of Cl^-.

Ionic liquids are often called the designer solvent. They can be designed by combination of anion and cation, and each of them has different physical properties. Taking advantage of this character of ionic liquids, some suitable ionic system may be chosen depending on the measurements.

I-4. Studies on Polysaccharides Other than Cellulose

Conformational studies on the cellulose derivatives have also been carried out in terms of molecular characteristics and solution behavior in various solvents, and thus expected to be a good standard for solution analysis of cellulose[19,25,26)]. Yanagisawa and Isogai[19)] compared the conformation of cellulose tris(phenylcarbamate) (CTC) dissolved in THF with that of cellulose in LiCl/amide solution. They concluded that cellulose and CTC take essentially identical conformation, behaving a typical semi-flexible chain in good solvent. Judging from their persistence length, CTC in THF (q =12 nm) has slightly higher rigidity than cellulose in LiCl/amide solution (q = 9 nm).

Comparison of the molecular characteristics between cellulose and other polysaccharide has also been paid attention. In particular, it makes possible to discuss the effect of position of glycosidic linkage on the chain conformation by studying systematically on the characteristics of the linear polysaccharides such as curdlan, amylose, and pullulan, having the same glucose residue as cellulose but different linkage. Chemical structures of these polysaccharides are shown in Figure I-2. Curdlan, consisting of β(1→3) glucosidic linkage, differs from cellulose respect to only in the linkage position. Hirano et al. compared curdlan with cellulose in terms of the z-average mean-square radius of gyration $\langle S^2\rangle_Z^{1/2}$ and the intrinsic viscosity $[\eta]$27). Pullulan is a water soluble polysaccharide, and thus well characterized by light scattering measurement. From the results of long years study, pullulan is considered as a flexible polysaccharide28,29).

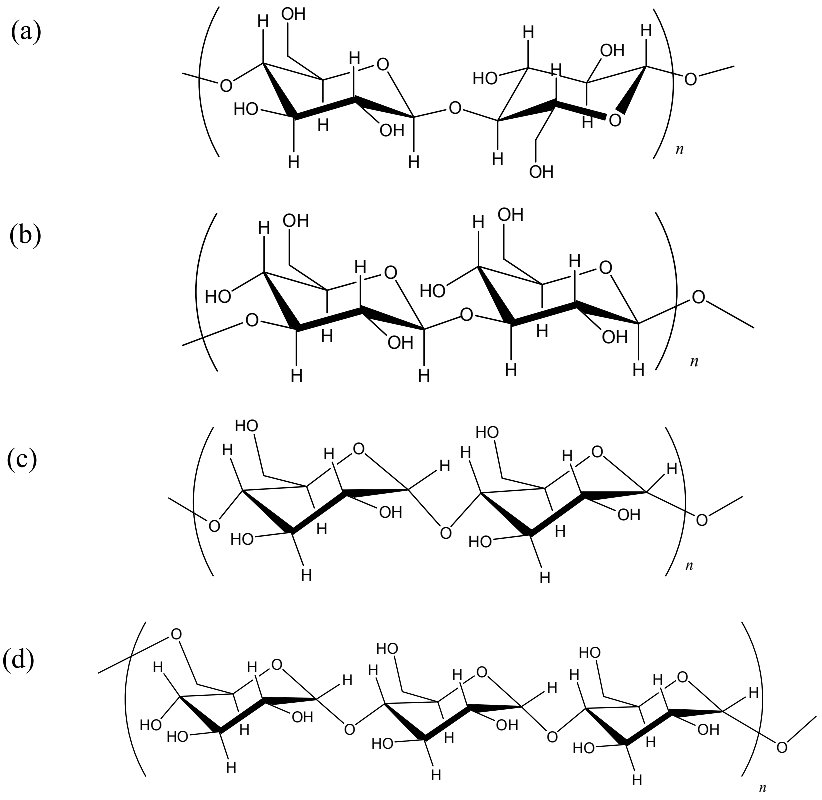

Figure I-2. Chemical structures of (a) cellulose (b) curdlan (c) amylose, and (d) pullulan.

I-5. Study on Polymer Chain Dynamics – Rheo-Optical Method

This thesis work applied the rheo-optical method to estimate the dynamic chain rigidity of cellulose and related polymers in solution and also in melt. This method is based on the following theoretical background.

For the case of rubbery materials, the strain-induced birefringence can be related to the stress through the stress-optical rule, SOR. The SOR can be derived from molecular theory30). The SOR indicates that both the stress and birefringence are originated from the segment orientation. However, the rule does not hold valid in the glassy zone because the glassy stress contributes to both the stress and birefringence. The relationship between stress and birefringence for amorphous polymers can be described with the modified stress optical rule, MSOR, over a wide time/ frequency region covering the terminal flow to the glassy zone31). The MSOR says that both of the stress and birefringence are composed of the rubbery and the glassy component and that the ordinary stress-optical rule holds well separately for each component. For the case of oscillatory tensile strain, the rule can be written as follows.

$$E^*(\omega) = E_R^*(\omega) + E_G^*(\omega) \qquad \text{(I-3)}$$

$$O^*(\omega) = C_R\, E_R^*(\omega) + C_G\, E_G^*(\omega) \qquad \text{(I-4)}$$

Here, $E^*(\omega) \equiv E'(\omega) + iE''(\omega)$ and $O^*(\omega) \equiv O'(\omega) + iO''(\omega)$ are complex Young's modulus and complex strain-optical coefficient, defined as a complex ratio of birefringence to strain. Subscripts R and G stand for rubber and glass. C is the associating stress-optical coefficient being independent of frequencies, ω. At low frequencies or at high temperatures, the G component has relaxed and therefore eqs I-3 and 4 are reduced to the ordinary stress-optical rule; $O^*(\omega) = C_R\, E_R^*(\omega)$. At high frequencies or at low temperatures, the relaxation of the R component would be frozen, and hence $E_R''(\omega) \sim 0$. Therefore, C_G is defined as follows.

$$C_G = \lim_{\omega \to \infty} \frac{O''(\omega)}{E''(\omega)} \tag{I-5}$$

Since the C_R is the ordinary stress-optical coefficient for rubbery materials, the R component reflects the reorientation process of segments after deformation. The limiting modulus at high frequency for the R component, $E_R'(\infty)$, can be related with the molar mass of the Rouse segment size, M_s32).

$$M_S = \frac{3\rho RT}{E_R'(\infty)} \tag{I-6}$$

Here, R is the gas constant. Rouse segment size can be considered as dynamical chain rigidity obtained by the Rheo-Optical method based on MSOR analysis. Inoue showed that the Rouse segment size is in accord with the Kuhn segment size (twice value of the persistence length, *static* rigidity) in melt.33) Peterson et al. estimated the Rouse segment size of polystyrene in Aroclor 1248.34) They reported the result that the Rouse segment in dilute solutions increased with decreasing concentration of solution. The estimated Rouse segment size was almost 5 times larger than Kuhn segment size at dilute concentration, but experimental interpretation has not been made so far.

I-6. Scope of this work

The aim of this thesis is to clarify relation between the static and dynamic chain rigidities of the cellulose chain. Taking into account of many academic and industrial advantages, ionic liquids are utilized as solvent for cellulose in this thesis work. Light scattering measurements were performed for cellulose/ionic liquid solutions to discuss the static chain rigidity. Moreover, using rheo-optical method mentioned above, the dynamic chain rigidity was estimated. The comparison of the static and dynamic chain rigidities makes it possible to understand the interrelation between the conformation and dynamics of cellulose chain in ionic liquids comprehensively.

Unfortunately, Rheo-optical measurements on cellulose in bulk are impossible because of the strong intermolecular interaction. Thus, the corresponding measurements were carried out on some cellulose derivatives in bulk and combined with the results for cellulose in solution to discuss the concentration dependence of the dynamic chain rigidity of the cellulose backbone over a wide concentration range. Moreover, the effect of the polymer chain stiffness on the relation between the conformation and dynamics of the polymer chain was examined by comparing the relation for cellulose with those for some other polysaccharides with the different glycosidic linkage type.

This thesis consists of the following chapters:

Chapter II describes the light scattering study on cellulose in ionic liquids. I encountered several difficulties at light scattering measurements on ionic liquid solutions. To escape the difficulties, I searched for suitable ionic liquids. It is worth noting that this is the first reliable light scattering study on ionic liquid solutions. In order to discuss the conformation-dynamics relation for polysaccharides other than cellulose, light scattering measurements were made also on pullulan and curdlan in an ionic liquid. Those results are also described in Chapter II.

Chapter III deals with simultaneous measurements of the dynamic viscoelasticity and birefringence, performed on cellulose/ionic liquid systems. From these measurements, the Rouse segment size reflecting the dynamic chain rigidity was obtained to discuss the relationship between the dynamic and static rigidities. The discussion is also given in this chapter.

The rheo-optical method was applied to also two kinds of cellulose derivatives, cellulose acetate propionate and cellulose acetate butyrate in bulk, of which results are described in Chapter IV. The dynamical chain rigidity for the cellulose derivatives in bulk was estimated to be compared with that for cellulose in solution.

Chapter V describes rheo-optical measurements carried out on ionic liquid solutions of pullulan and amylose. Concentration dependences of the Rouse segment size for pullullan and amylose in an ionic liquid are compared with that for cellulose in the same solvent.

Finally, in Chapter VI, main results and conclusions of this work are summarized.

References

1) Chu, S. S. C.; Jeffrey, G. A. *Acta Cryst.* **1968**, B24, 830.

2) Goebel, K. D.; Harvie, C. E.; Brant, D. A. *Appl. Polym. Symp.* **1976**, 28, 671

3) Sato, T.; Terao, K.; Teramoto, A.; Fujiki, M. *Polymer* **2003**, 44, 5447.

4) Sato, T.; Terao, K.; Teramoto, A.; Fujiki, M. *Macromolecules* **2002**, 35, 2141.

5) Mansfield, M. L. *Macromolecules* **1986**, 19, 854.

6) Yanai, H.; Sato, T. *Polym. J.* **2006**, 38, 226.

7) Goebel, C. V.; Dimpfl, W. L.; Brant, D. A. *Macromolecules* **1970**, 3, 644.

8) Brant, D. A.; Dimpfl, W. L. *Macromolecules* **1970**, 3, 655.

9) Nakata, Y.; Kitamura, S.; Takeo, K.; Norisuye, T. *Polym. J.* **1994**, 26, 1085.

10) Chu, S. S. C.; Jeffrey, G. A. *Acta Cryst.* **1967**, 23, 1038.

11) Burton, B. A.; Brant, D. A. *Biopolymers* **1983**, 22, 1769.

12) Jordan, R. C.; Brant, D. A.; Cesaro, A. *Biopolymers* **1978**, 17, 2617.

13) Fujii, M.; Nagasaka, K.; Shimada, J.; Yamakawa, H. *Macromolecules* **1983**, 16, 1613.

14) Schweizer, E. J. *J. Prakt. Chem.* **1857,** 72,109.

15) McCormick, C. L.; Callais, P. A.; Hutchinson, B. H. *Macromolecules* **1985,** 18, 2394.

16) Henley, D. *Ark. Kemi* **1961,** 18, 327.

17) Brown, W.; Wikström, R. *Eur Polym J* **1965,** 1, 1.

18) Saalwächter, K.; Burchard, W. *Macromolecules* **2001,** 34, 5587.

19) Yanagisawa, M.; Isogai, A. *Biomacromolecules* **2005,** 6, 1258.

20) Swatloski, R. P.; Spear, S. K.; Holbrey, J. D.; Rogers, R. D. *J. Am. Chem. Soc.* **2002,** 124, 4974.

21) Kuang, Q.; Zhao, J.; Niu, Y.; Zhang, J.; Wang, Z. *J. Phys. Chem. B.* **2008,** 112, 10234.

22) Horinaka, J.; Yasuda, R.; Takigawa, T. *J. Polym. Sci. B. Polym. Phys* **2011,** 49, 961.

23) Chen, Y.; Zhang, Y. M.; Ke, F. Y.; Zhou, J. H.; Wang, H. P.; Liang, D. H. *Polymer* **2011,** 52, 481.

24) Chen, X.; Zhang, Y.; Wang, H.; Wang, S.-W.; Liang, S.; Colby, R. H. *J. Rheol.* **2011,** 55, 485.

25) Kasabo, F.; Kanemitsu, T.; Nagasawa, T.; Sato, T.; Teramoto, A. *Macromolecules* **2000,** 33, 2748.

26) Kamide, K.; Saito, M.; Suzuki, H. *Makromol. Chem., Rapid Commun.* **1983,** 4, 33.

27) Hirano, I.; Einaga, Y.; Fujita, H. *Polym. J.* **1979,** 11, 901.

28) Kato, T.; Okamoto, T.; Tokuya, T.; Takahashi, A. *Biopolymers* **1982,** 21, 1623.

29) Kato, T.; Katsuki, T.; Takahashi, A. *Macromolecules* **1984,** 17, 1726.

30) Doi, M.; Edwards, S. F. *The Theory of Polymer Dynamics,* Clarendon: Oxford, 1986, p. 391.

31) Inoue, T.; Okamoto, H.; Osaki, K. *Macromolecules* **1991**, 24, 5670.

32) Inoue, T.; Osaki, K. *Macromolecules* **1996**, 29, 1595.

33) Inoue, T. *Macromolecules* **2006**, 39, 4615.

34) Peterson, S. C.; Echeverria, I.; Hahn, S. F.; Strand, D. A.; Schrag, J. L. *J. Polym. Sci. B. Polym. Phys* **2001,** 39, 2860.

Chapter II. Conformation of the Cellulose Chain in Ionic Liquids

II-1. Introduction

As mentioned in the previous chapter, the main purpose of this thesis is to elucidate the relation between the static and dynamic chain rigidities of cellulose in solution. To do so, one has to determine both chain rigidities in the same solvent. However, this is not easy task because of the opposite requirement on the solvent for the two rigidity measurements: the solvent viscosity must be low for the static rigidity measurements, but it has to be high for the dynamic rigidity measurements.

In the present thesis, I focused on ionic liquids, because some ionic liquids possess intermediate viscosities which may make both rigidity measurements possible. This Chapter describes the conformational study on cellulose in ionic liquids to estimate the static chain rigidity.

The conformation of the polymer chain in solution is usually analyzed in terms of the wormlike-chain model, which is characterized by two parameters, the persistence length q and the contour length L. The former expresses the static chain rigidity. To determine this parameter, one must measure the chain dimension, e.g., the hydrodynamic radius R_{H}, and the molecular weight M, which is related to L by $L = M/M_{\mathrm{L}}$ with the molecular weight per unit contour length M_{L}.

I have selected the light scattering technique to measure both R_{H} and M in this study. However, there were following difficulties in the light scattering measurements on ionic liquid solutions of cellulose:

(1) Refractive indices n_0 of ionic liquids are considerably high, which decrease the refractive index increment $\partial n/\partial c$ or the light scattering power of cellulose in the ionic liquids.

The low scattering power makes difficult precise light scattering measurements on dilute solutions.

(2) Many ionic liquids contain a small amount of impurities which emit fluorescence. Since the ionic liquids are hardly volatile and re-crystallized, the impurities are difficult to be removed from the ionic liquids. Fluorescence light from the solvent is so strong that precise light scattering measurements are not easy.

(3) Some ionic liquids are too viscous to make optical purification of test solutions for light scattering measurements.

The present study examined the following four ionic liquids, of which liquid states are stable at room temperature; (a) 1-Allyl-3-methylimidazolium Chloride (AmimCl), (b) 1-butyl-3-methylimidazolium Chloride (BmimCl), (c) 1-ethyl-3-methylimidazolium dimethyl phosphate (EmimDMP), and (d) 1-ethyl-3- methylimidazolium methyl phosphonate (EmimMP). The chemical structures of the four ionic liquids are given in Figure II-1, and their viscosity coefficients η_0 and refractive indices n_0 are listed in Table II-1. The values of η_0 and n_0 of BmimCl are too high to use for light scattering measurements because of the above difficulties (1) and (3). Several cellulose samples with different molecular weight were used in this study in order to investigate the molecular weight dependence of the hydrodynamic radius.

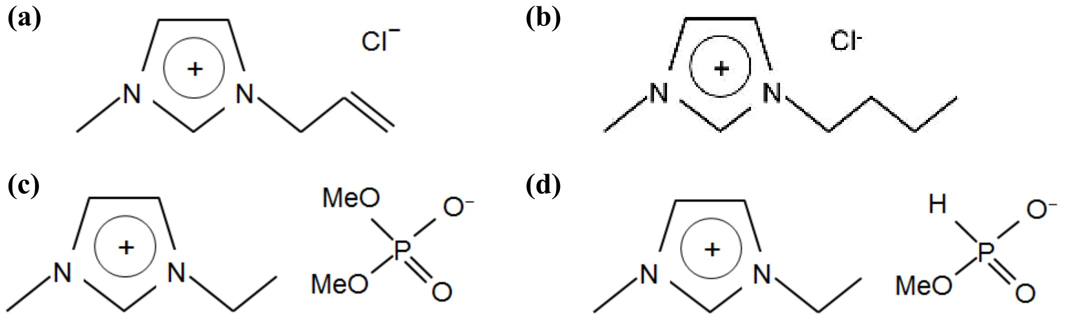

Figure II-1. Chemical structures of the ionic liquids. (a) AmimCl, (b)BmimCl, (c) EmimDMP, and (d) EmimMP.

Table II-1. Physical properties of four ionic liquids examined in this study.

Ionic liquids	n_0	η_0 / mPas	ρ / gcm^{-3}	$\partial n/\partial c$[*]
BmimCl	1.551[**]	3950 (30°C)[**]	1.08[***]	–
AmimCl	1.546[**]	1150 (30°C)[**]	1.17	–
EmimDMP	1.48	154 (25°C)	1.16	0.0997
EmimMP	1.49	77.8 (25°C)	1.14	0.0727

[*] Refractive index increment of cellulose in the ionic liquid. [**] Taken from the reference 1).

[***] Taken from the reference 2).

II-2. Experimental

Materials and Preparation of Solutions. Two different cotton linter cellulose samples (CC1, CC2) and a regenerated cellulose sample, cupra (CP), were used for light scattering measurements. Samples CC1 and CP were supplied from Asahi Kasei Medical, while CC2 was kindly supplied by Prof. Hiroyuki Yano (Kyoto University). A pullulan sample (Hayashibara) was also kindly supplied by Prof. T. Shikata (Tokyo University of Agriculture and Technology). A curdlan sample was purchased from Wako Pure Chemical Industries, Ltd.

The ionic liquids listed in Table II-1 were used in this study. AmimCl and EmimDMP were purchased from Sigma Aldrich, BmimCl from Wako, and EmimMP from Kanto Chemical Co., Inc., and were used without further purification. According to manufacturing sheet, the purity of ionic liquids are 99.4 % for AmimCl and EmimDMP and 99.886% for EmimMP. All ionic liquids were dried in a vacuum oven at 60 ˚C. Then, dried cellulose sample was dissolved into the ionic liquids in vacuum state at 80 ˚C (in AmimCl), 75 ˚C (in EmimDMP), and 65 ˚C (in EmimMP) respectively for 24 hours.

Fluorescence Measurements. Steady-state fluorescence spectra for the four ionic liquids irradiated by excitation light of 532nm were recorded on a Hitachi F–4500 fluorescence spectrometer at room temperature. The slit widths for excitation and emission sides were kept at 2.5 nm and 1.0 nm during measurements.

Specific Refractive Index Increment Measurements. Specific refractive index increments ($\partial n/\partial c$) for ionic liquid solutions of cellulose were measured using a modified Schulz–Cantow type differential refractometer (Shimazu) with 488 and 546 nm wavelength light at 25.0 °C. Values of $\partial n/\partial c$ at λ_0 (wavelength) = 532 nm were obtained by interpolation of $\partial n/\partial c$ values at λ_0 = 488 and 546 nm to be 0.0997 cm^{3}g^{-1} for EmimDMP and 0.0727 cm^{3}g^{-1} for EmimMP, but it was impossible to measure $\partial n/\partial c$ for AmimCl solutions, because the refractive index of AmimCl was so large that the incident beam was totally reflected at the cell wall. Values of ($\partial n/\partial c$) for pulullan and curdlan are assumed to be equal to that for cellulsoe.

Light Scattering Measurements. Test solutions for light scattering measurements were optically cleaned by filtration through a nylon membrane filter with a pore–size of 0.8 μm.

Simultaneous static and dynamic light scattering measurements were carried out for cellulose, pulullan, and curdlan solutions using ALV/SLS/DLS–5000 light scattering instrument equipped with an ALV–5000 multiple τ digital correlator. Vertically polarized light with the wavelength of λ_0 = 532 nm emitted from an Nd:YAG laser was used as an incident light. In order to cut off the fluorescence from the solutions, a band–pass filter at 532 nm (Edmund Optics: half bandwidth = 10 nm) was equipped in front of the detector of the scattered light for the measurements of EmimDMP and EmimMP solutions. The light scattering system was calibrated using toluene as the reference material. The Rayleigh ratio of toluene R_{tol} for vertically polarized 532 nm light was taken to be 2.72×10^{-5} cm^{-1} at 25 °C. The excess Rayleigh ratio R_θ at scattering angle θ of each solution over that of the solvent was calculated from the scattering intensity of the solution $I_{\theta,\mathrm{soln}}$ and solvent $I_{\theta,\mathrm{solv}}$ by the standard procedure$^{3)}$. The intensity auto-correlatiuon function $g^{(2)}(t)$ obtained by dynamic light scattering was analyzed by CONTIN to obtain the spectrum $A(\tau)$ of the relaxation time τ.

II-3. Results and discussion

II-3-1. Fluorescence Spectra for Ionic Liquids

Figure II-2 shows fluorescence spectra for the four ionic liquids, Amim Cl, BmimCl, EmimDMP, and EmimMP. The sharp peeks at λ (wavelength) = 532 nm observed for all ionic liquid are mostly originated from the Rayleigh scattering. BmimCl does not emit any fluorescence. However, BmimCl is not suitable for light scattering measurement because of its high viscosity. On the other hand, fluorescence was more or less observed at $\lambda > 530$ nm for AmimCl, EmimDMP, and EmimMP, and that from AmimCl is the strongest. Fluorescence observed at $\lambda > 500$ nm should be originated from impurity in the ionic liquids, because fluorescence is not expected from the chemical structures of these ionic liquids. At present, I have no information about the impurities in the ionic liquids. Further purification of the ionic liquids has not made because no effective purification method has not established yet.

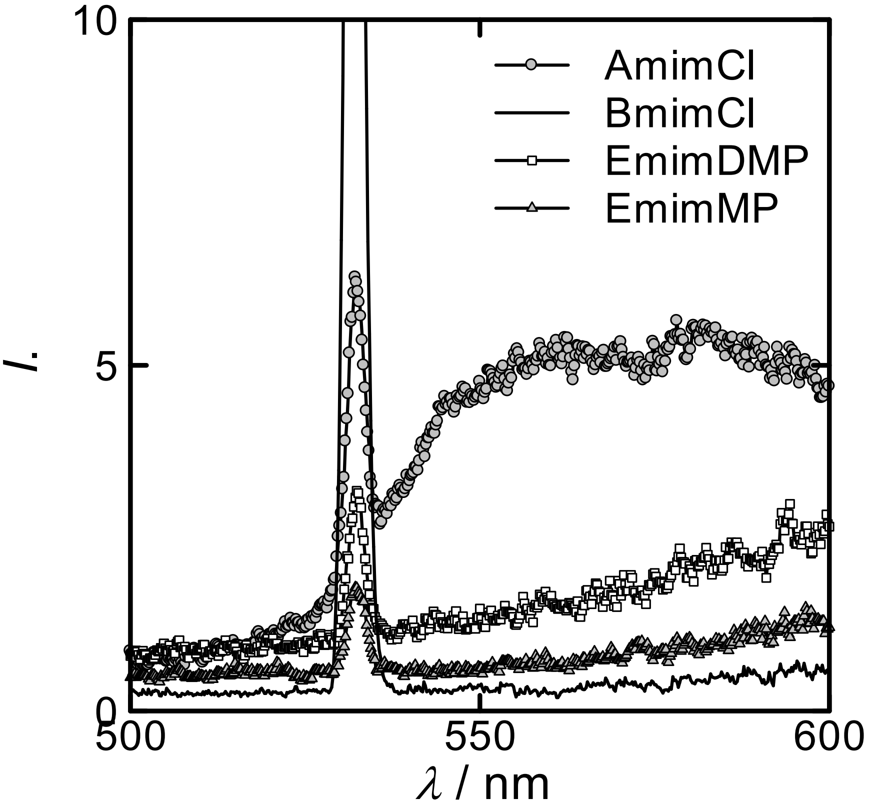

Figure II-2. Fluorescence spectra for ionic liquids.

II-3-2. Light Scattering Results for Cellulose in Ionic Liquids

Solutions of AmimCl. Figure II-3 shows angular dependences of R_θ for three CC1/AmimCl solutions of the sample CC1 at 25 °C. The angular dependence becomes stronger with increasing concentration, c, and R_θ for solutions at c = 2.92 and 5.80 /10^{-3}g cm^{-3} take negative values at higher k^2. The negative R_θ may come from fluorescence emitting from impurity in the solvent AmimCl, which reduces with decreasing the impurity concentration or increasing the polymer concentration c. The strong k dependence indicates that the solutions contain large aggregates of cellulose molecules. It was difficult to analyze the R_θ data to obtain the weight average molecular weight M_w for the AmimCl solutions.

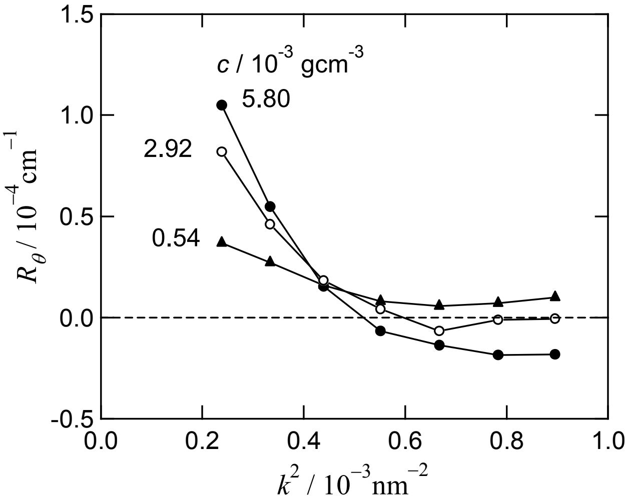

Figure II-3. Angular dependences of R_θ for three AmimCl solutions of CC1.

Solutions of EmimMP. EmimMP has a lower viscosity and a lower refractive index as well as higher purity than AmimCl, and R_θ in EmimMP solution of cellulose was positive over the whole angular range and c (< 0.01 g/cm^3) examined. In order to cut off the fluorescence from the solvent, a band–pass filter at 532 nm was placed in front of light detector. Figure II-4(a) displays plots of Kc/R_θ against k^2 for EmimMP solutions of CC1. K is the optical constant. The angular dependence of Kc/R_θ is strong especially for higher c.

Dynamic light scattering measurements on the same solutions provided bimodal or tri-modal relaxation time spectra $A(\tau)$. The spectra for a solution of c = 0.00855 g/cm^3 are shown in Figure II-4(b). The common peak at $k^2\tau > 5 \times 10^{14}$ is regarded as large aggregating components of cellulose chains. Since I am interested in molecularly dispersed cellulose chains in the ionic liquid, the scattering component of the rightmost peak should be eliminated from the total R_θ, using the equation

$$R_{\theta,\mathrm{fast}} = R_\theta \left[1-\int_{\mathrm{slow}} A(\tau)\mathrm{d}\tau \Big/ \int_{\mathrm{all}} A(\tau)\mathrm{d}\tau\right] \quad \text{(II-1)}$$

where the integral in the numerator was taken over the rightmost peak, and I call the fast-relation component of R_θ as $R_{\theta,\mathrm{fast}}$. When spectra are tri-modal, $R_{\theta,\mathrm{fast}}$ contains the first and second peak components of $A(\tau)$. The CONTIN analysis is susceptible to noise in the time-correlation function $g^{(2)}(t)$, which may provide some ghost middle component peak of $A(\tau)$. Therefore, details of the middle peak component are not discussed.

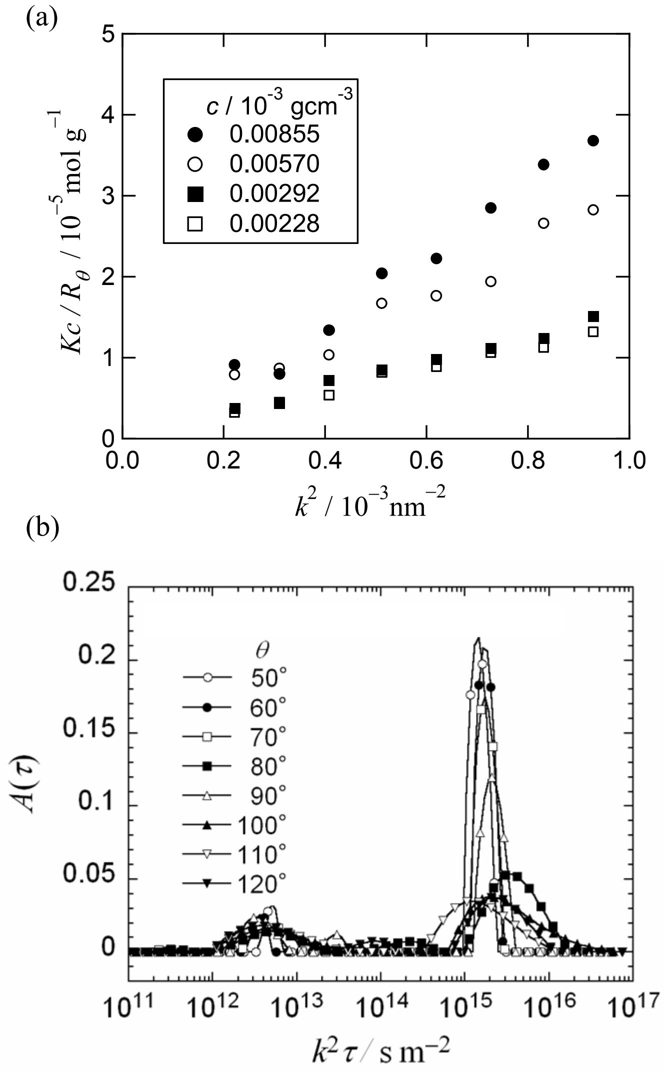

Figure II-4. (a) Angular dependences of Kc/R_θ for three EmimMP solutions of CC1. (b) Relaxation time spectra $A(\tau)$ for a EmimMP solution of CC1 of $c = 0.00855$ g/cm^3.

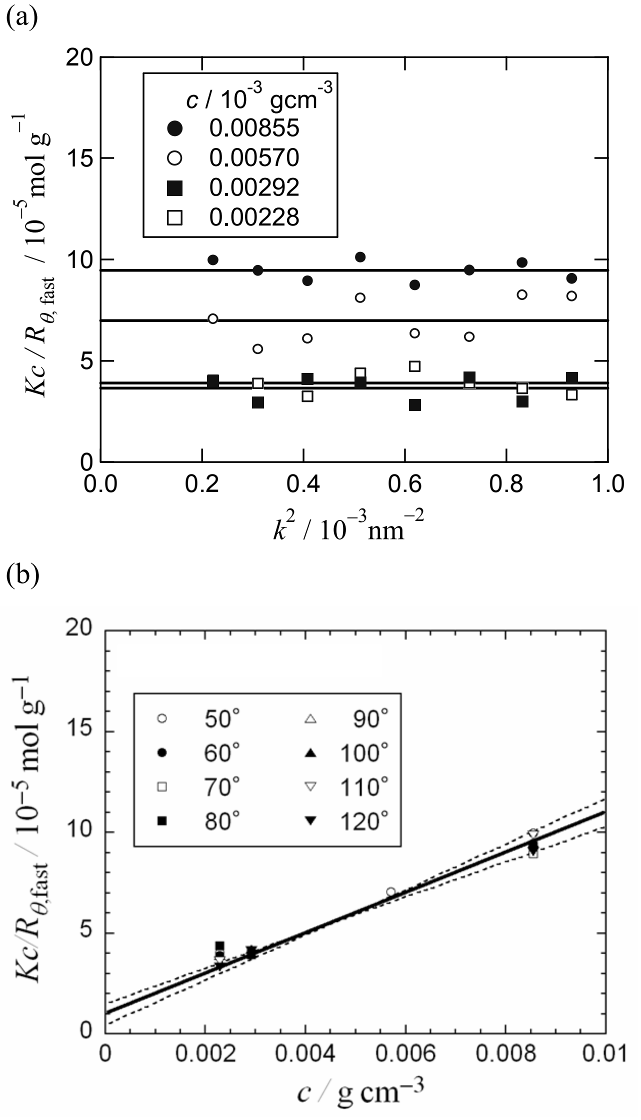

Figure II-5. Angular and concentration dependences of $Kc/R_{\theta,\mathrm{fast}}$ for CC1 in EmimMP.

Figure II-5 shows the angular and concentration dependences of $Kc/R_{\theta,\mathrm{fast}}$ for CC1 in EmimMP. In Panel (a), data points are more or less scattered, and appreciable angular dependence is not observed in a contrast to Kc/R_θ in Figure II-4 (a), indicating that the molecularly dispersed chain dimension of the CC1 sample is much smaller than the wavelength of the light (532 nm). On the other hand, the concentration dependence of $Kc/R_{\theta,\mathrm{fast}}$ in Figure II-5 (b) is quite strong, which makes difficult to extrapolate $Kc/R_{\theta,\mathrm{fast}}$ to the zero c to accurately estimate the molecular weight. Panel (b) plots only the data points with small deviations from the average value in each c in Panel (a). Assuming that $Kc/R_{\theta,\mathrm{fast}}$ is independent of θ, I extrapolate $Kc/R_{\theta,\mathrm{fast}}$ to the zero c along the dotted lines. It is noted that the linearity of the Zimm plot with respect to the c dependence is better than that of the Berry plot for stiff-chain polymers, like cellulose$^{4)}$. The weight average molecular weight $M_{\mathrm{w,fast}}$ and the second virial coefficient $A_{2.\mathrm{fast}}$ of the fast-relaxation component were estimated using

$$\frac{Kc}{R_{\theta,\mathrm{fast}}} = \lim_{\theta \to 0} \frac{Kc}{R_{\theta,\mathrm{fast}}} = \frac{1}{M_{\mathrm{w,fast}}} + 2A_{2,\mathrm{fast}}c \quad \text{(II-2)}$$

by assuming a small amount of the slow-relaxation component. The values of $M_{\mathrm{w,fast}}$ and $A_{2.\mathrm{fast}}$ estimated from the dotted lines in Figure II-5(b) range from 5.6×10^4 to 1.7×10^5 and from 4.3×10^{-3} to 5.6×10^{-3} cm^{3}g^{-2}mol, respectively. The large uncertainty in $M_{\mathrm{w,fast}}$ arises from the strong c dependence of $Kc/R_{\theta,\mathrm{fast}}$, as indicated by the $A_{2,\mathrm{fast}}$ values.

From $A(\tau)$ shown in Figure II-4(b), I estimated the first cumulant of the fast-relaxation component Γ_{fast} using the equation

$$\Gamma_{\mathrm{fast}} = \int_{\mathrm{fast}} \tau^{-1} A(\tau)\mathrm{d}\tau \Big/ \int_{\mathrm{all}} A(\tau)\mathrm{d}\tau \qquad \text{(II-3)}$$

where the integral in the numerator is taken over τ corresponding to the fast-relaxation component. Figure II-6 shows the concentration dependence of $(6\pi\eta_{\mathrm{S}}/k_{\mathrm{B}}T)(\Gamma_{\mathrm{fast}}/k^2)$ for CC1 in EmimMP, where η_{S} is the solvent viscosity and $k_{\mathrm{B}}T$ is the Boltzmann constant multiplied by the absolute temperature. Again, the data points at different θ are considerably scattered, but any systematic angular dependence of $\Gamma_{\mathrm{fast}}/k^2$ is not observed. By extrapolation along the dotted lines in the figure, the hydrodynamic radius of the fast-relaxation component $R_{\mathrm{H,fast}}$ was estimated using the equation

$$R_{\mathrm{H,fast}}{}^{-1} = \frac{6\pi\eta_{\mathrm{S}}}{k_B T}\frac{\Gamma_{\mathrm{fast}}}{k^2} \qquad \text{(II-4)}$$

The obtained $R_{\mathrm{H,fast}}$ ranges from 15 to 29 nm.

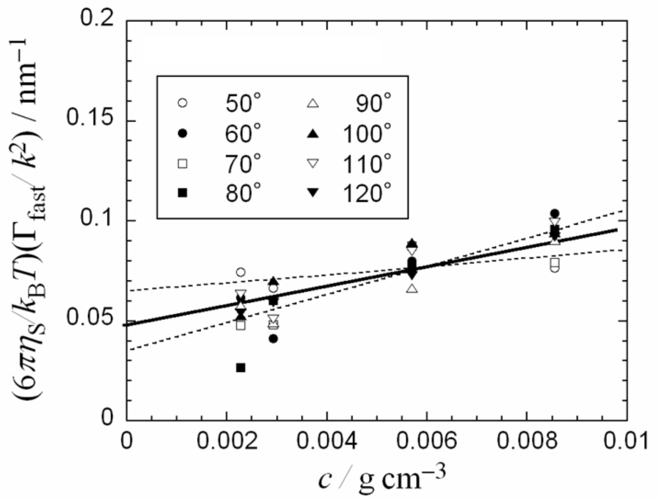

Figure II-6. Concentration dependence of $(6\pi\eta_{\mathrm{S}}/k_{\mathrm{B}}T)(\Gamma_{\mathrm{fast}}/k^2)$ for CC1 in EmimMP.

Similar static and dynamic light scattering results were obtained for EmimMP solutions of the cellulose sample CC2, as well as EmimDMP solutions of the cellulose samples CC1, CC2, CP and the samples of curdlan and pullulan.

II-3-3. Conformation of the Cellulose Chain in EmimMP and EmimDMP

Molecular Weights, Second Virial Coefficients, and Hydrodynamic Radii. Static and dynamic light scattering data were collected for dilute EmimMP and EmimDMP solutions of three different cellulose samples, CC1, CC2, and CP, and the data obtained were analyzed in the same way as described above. Geometric averages of the maximum and minimum values obtained for $M_{\mathrm{w,fast}}$, $A_{2,\mathrm{fast}}$, and $R_{\mathrm{H,fast}}$ are listed in Table II-2, and the double logarithmic plot of $R_{\mathrm{H,fast}}$ against $M_{\mathrm{w,fast}}$ is shown in Figure II-7. Both results of $M_{\mathrm{w,fast}}$ and $R_{\mathrm{H,fast}}$ have large error bars, due to uncertainties at the concentration extrapolation, as mentioned above,. Both $M_{\mathrm{w,fast}}$ and $R_{\mathrm{H,fast}}$ are not so much dependent on the cellulose samples and nor so much on the solvents. On the other hand, $A_{2,\mathrm{fast}}$ of cellulose in EmimDMP is almost twice as large as that in EmimMP. The large A_2 may come from the fluorescence of the solvents, which was not completely cut by the band-pass filter used at light scattering experiment.

Table II-2. The light scattering results of $M_{\mathrm{w,fast}}$, $A_{2,\mathrm{fast}}$, and $R_{\mathrm{H,fast}}$ for cellulose samples in ionic liquid solutions.

Solution	$M_{\mathrm{w,fast}}$ / 10^5	$A_{2,\mathrm{fast}}$ / 10^{-3} cm^{3}g^{-2}mol	$R_{\mathrm{H,fast}}$ / nm
CC1 / EmimMP	1.3	5.0	21
CC2 / EmimMP	1.4	7.0	17
CC1 / EmimDMP	1.6	12	20
CC2 / EmimDMP	1.4	11	20
CP / EmimDMP	1.3	13	19

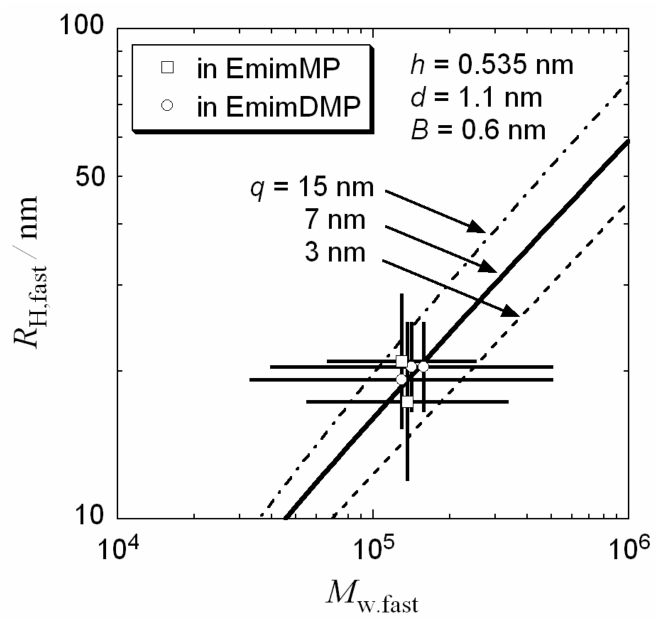

Figure II-7. The double logarithmic plot of $R_{\mathrm{H,fast}}$ against $M_{\mathrm{w,fast}}$.

Analysis by the Wormlike Chain Model. The molecular weight dependence of the hydrodynamic radius can be analyzed using the wormlike cylinder model, which is characterized in terms of the persistence length q, the contour length L, the diameter d, and the excluded-volume strength per unit contour length B. On the other hand, the molecular weight $M_{\mathrm{w,fast}}$ and the hydrodynamic radius $R_{\mathrm{H,fast}}$ are simply denoted as M and R_{H}, respectively, and polydispersity effects on M and R_{H} are not considered in what follows.

Yamakawa, Fujii, and Yoshizaki calculated the translational diffusion coefficient or the hydrodynamic radius $R_{\mathrm{H,0}}$ for the unperturbed wormlike cylinder as a function of q, L, and d. The explicit functional form is given in literatures5-8). On the other hand, the perturbed hydrodynamic radius R_{H} is calculated by

$$R_{\mathrm{H}} = \alpha_{\mathrm{H}}(\tilde{z}) R_{\mathrm{H,0}} \tag{II-5}$$

where $\alpha_{\mathrm{H}}(\tilde{z})$ is the expansion factor for R_{H} due to the excluded volume effect, given by a function of the scaled excluded volume parameter $\tilde{z}$. The parameter $\tilde{z}$ can be calculated by

$$\tilde{z} = \frac{3}{4} K(N_{\mathrm{K}}) \cdot \left(\frac{3}{2\pi} \right)^{3/2} \frac{B}{2q} N_{\mathrm{K}}^{1/2} \qquad \text{(II-6)}$$

where N_{K} is the number of Kuhn's segments per chain calculated by $N_{\mathrm{K}} = L/2q$, and $K(N_{\mathrm{K}})$ is a known function of N_{K}. Explicit functional forms of $\alpha_{\mathrm{H}}(\tilde{z})$ and $K(N_{\mathrm{K}})$ are given in literatures[9-11)].

The contour length L is calculated from the experimentally obtained molecular weight M by

$$L = \frac{M}{M_0} h \qquad \text{(II-7)}$$

with the molecular weight M_0 and the contour length h of the monomer unit. For cellulose, $M_0 = 162$ and $h = 0.535$ nm. Therefore, unknown parameters in the above equations to calculate the M dependence of R_{H} are q, d, and B. Since the molecular weight range of the data points in Figure II-7 is not wide, it was difficult to determine the three parameters uniquely. Thus, values of d and B of cellulose in EmimMP and EmimDMP are assumed to be approximately identical with those in cadoxen. Cadoxen is another good solvent for cellulose, and the molecular weight dependence of the intrinsic viscosity for cellulose was studied in this solvent over a wide molecular weight range. As mentioned in Appendix, d and B of cellulose were determined to be 1.1 nm and 0.6 nm, respectively, in cadoxen.

In Figure II-7, the solid, dashed, and dash-dot curves indicate theoretical values calculated by the above theory with q = 7 nm, 3 nm, and 15 nm, respectively, at d and B fixed to be 1.1 nm and 0.6 nm, respectively. Although experimental errors in M and R_H are considerably large, the best fit is obtained at q = 7 nm in EmimMP and EmimDMP.

The conformation of the cellulose chain has previously been investigated in DMAc/LiCl, cadoxen, Cd-tren, and aqueous LiOH with urea. The wormlike cylinder parameters estimated in the solvents are listed in Table II-3, along with the results in the ionic liquids obtained in this study. Furthermore, Table II-3 includes the wormlike cylinder parameters of cellulose derivatives.

Table II-3. The model parameters (q, d, and B) of cellulose and cellulose derivative in various solutions.

Polymer	Solvent	q / nm	d / nm	B / nm	Method	Reference
cellulose	EmimMP & EmimDMP	7	1.1 [a]	0.6 [a]	R_H	This study
	cadoxen	4	1.1	0.6	$[\eta]$	12)
	Cd-tren	7.9			R_H	13)
	aqueous LiOH/Urea	6.1			$[\eta]$	14)
	DMAc with LiCl	9.0			$\langle S^2 \rangle$	15)
CTC [b]	THF	10.5	1.8	1.8	$\langle S^2 \rangle$,[c] R_H, $[\eta]$	4)
CAP [d]	dimethyl phthalate	5.9			$[\eta]$	16)
HPC [e]	DMAc	6.5			$[\eta]$	17)
CTA [f]	trifluoroacetic acid	5.3			$[\eta]$	18)

[a] Assumed value. [b] cellulose tris(phenylcarbamate). [c] square radius of gyration. [d] cellulose acetate propionate. [e] (hydroxypropyl)cellulose. [f] cellulose triacetate

The Static Chain Rigidity of Cellulose in Ionic Liquids. As shown in Figure I-3, the conformation of the cellulose chain is determined by the two torsional angles ϕ and ψ. Brant et al. calculated the internal rotation energy, and concluded that a left-handed nearly 3/1 and a nearly 2/1 helical conformations are the energetically most stable states and the sequence of the two helical states provides an extended conformation of the cellulose chain$^{19)}$. The persistence length q they calculated from the internal rotation energy was as large as 30 nm at 25 °C, but experimental q values for cellulose and its derivatives, listed in Table II-3, are considerably smaller than this theoretical value.

Yanai and Sato proposed that the disagreement between the theoretical and experiment values of q can be explained by the kink conformation, which has a higher free energy G^* than the two stable helical states$^{20)}$. Such a kink conformation occurs when the glucosidic bond angle β (cf. Figure I-1) slightly deviates from the standard value, and a kink angle $\tilde{\theta}_{\mathrm{K}}$ of ca. 40° is introduced to the cellulose chain, as predicted theoretically by Brant et al. As the result, the cellulose chain is viewed as a broken wormlike chain, and its effective persistence length q is given by

$$\frac{1}{q}=\frac{1}{q_0}+\frac{1-\cos\tilde{\theta}_{\mathrm{K}}}{h\exp\left(G^*/RT\right)} \qquad \text{(II-8)}$$

where q_0 is the persistence length for the chain with no kink (= 30 nm at 25 °C), and RT is the gas constant multiplied by the absolute temperature.

When G^* is chosen to be 3.5 kJ/mol, eq II-8 provides the q value (= 7 nm) for cellulose in EmimMP and EmimDMP at 25 °C. The average number of glucose residues between neighboring kinks calculated by $\exp(G^*/RT)$ is ca. 4, so that the kink conformation appears rather frequently.

II-3-3. Conformation of Other Polysaccharides in Ionic Liquids

Same light scattering measurements and their data analysis were also carried out on EmimDMP solutions of curdlan and pullulan samples. The obtained $M_{\mathrm{w,fast}}$, $A_{2,\mathrm{fast}}$, and $R_{\mathrm{H,fast}}$ values are listed in Table II-4, and $R_{\mathrm{H,fast}}$ is plotted against $M_{\mathrm{w,fast}}$ in Figure II-8. Kato et al. reported the relation between R_{H} and M_{w} for pulullan in water. Figure II-8 also contains their data, indicated by small filled circles. These filled circles and the unfilled circle for pulullan in EmimDMP obey the same curve, indicating that the conformation of pulullan in EmimDMP may be identical with that in water.

Table II-4. The light scattering results of $M_{\mathrm{w,fast}}$, $A_{2,\mathrm{fast}}$, and $R_{\mathrm{H,fast}}$ for curdlan and pullulan in ionic liquid solutions.

Sample	Solvent	$M_{\mathrm{w,fast}}$ / 10^5	$A_{2,\mathrm{fast}}$ / 10^{-3} cm^{3}g^{-2}mol	$R_{\mathrm{H,fast}}$ / nm
Curdlan	EmimDMP	2.4	6.6	35
Pullulan	EmimDMP	3.2	8.4	16

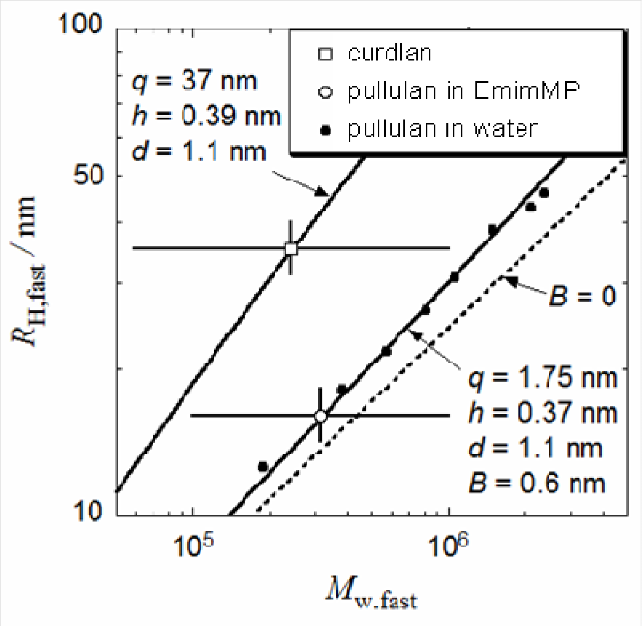

Figure II-8. Double logarithmic plot of $R_{H,fast}$ against $M_{w,fast}$ for curdlan and pullulan samples in EmimDMP. Literature data of pulullan in water are also plotted by small filled circles[21)].

The data points for pulullan in water are enough to determine the wormlike cylinder parameters by fitting the data points. The contour length h per monomer unit for pulullan is assumed to be identical with that (= 0.37 nm[22, 23)]) for amylose, because their molecular weight dependences of the intrinsic viscosity are close each other[21)]. The solid curve for pulullan in Figure II-8 shows the fitting result, and the derived parameters are listed in Table II-5. The persistence length q of pullulan is determined as 1.75 nm in water and EmimDMP, both of which are polar solvents. It is much smaller than that for cellulose in the same solvent, maybe because pulullan is an α-linked D-glucan.

Ochiai et al. studied dilute solution properties of curdlan tris(phenylcarbamate) (CdTPC) in THF, and determined the wormlike cylinder parameters[24)]. Their results are also listed in Table II-5. The persistence length of CdTPC, a β-glucan is larger than that of cellulose in various solvents. Although there is only one data point for curdlan in EmimDMP, h and d values may be selected from crystallographic data for curdlan tris(acetate) 25), to be 0.39 nm and 1.1 nm, respectively. Furthermore, if the curdlan chain is very stiff, the excluded volume effect is negligible, so that the data point can be compared with the unperturbed $R_{\mathrm{H},0}$ without including the parameter B. Therefore, the only fitting parameter q can be determined to agree $R_{\mathrm{H},0}$ with the experimental result. The obtained value of q was 37 nm, which is even higher than CdTPC in THF. It is noted that persistence lengths of curdlan in a cadoxen-water mixsture and in 0.3 M NaOH aqueous solution were reported to be 2.8 nm27) and 6.8 nm28), respectively. The obtained value of q in this study is appreciable higher compared with that in these solvents. This static rigidity may come from a locally helical structure of the curdlan chain even in an ionic liquid.

Table II-5. The model parameters (q, d, and B) for various solutions of pulluan, curdlan, and CsTPC.

Polymer	Solvent	q/nm	d/nm	B/nm	Method	Reference
pulullan	EmimDMP	1.75	1.1 [a]	0.5 [a]	R_{H}	This study
	water	1.75	1.1	0.5	R_{H}	21)
curdlan	EmimDMP	37	1.1 [b]	– [c]	R_{H}	This study
CdTPC [c]	THF	29	2.1	– [d]	$\langle S^2 \rangle$,[e] $P(k)$,[f] $[\eta]$	24)

[a] Assumed value. [b] Taken from crystallographic data for curdlan tris(acetate). [c] Curdlan tris(phenylcarbamate). [d] Too stiff to determine B. [e] Square radius of gyration. [f] Particle scattering function.

II-4. Conclusions

Ionic liquids available for light scattering measurements were searched for to use the conformation study of cellulose. Fluorescence was observed for AmimCl, EmimMP, and EmimDMP, because the impurity remained in the ionic liquids. Especially, AmimCl was unsuitable for the light scattering solvent, because fluorescence was too strong. Therefore, EmimMP and EmimDMP were used for solvents of the light scattering study.

The result of dynamic light scattering demonstrated that a small amount of large aggregates of cellulose chains coexist with the molecularly dispersed cellulose component in the ionic liquids. This aggregating component was eliminated from the total scattering intensity using the relaxation time spectrum obtained by dynamic light scattering to estimate the molecular weight of cellulose. Furthermore, the hydrodynamic radius of the molecularly dispersed cellulose component was estimated by dynamic light scattering. The molecular weight dependence of the hydrodynamic radius for cellulose in ionic liquids obtained was analyzed using the wormlike cylinder model to estimate the static chain rigidity or the persistence length of cellulose in ionic liquids. The persistence length obtained was compared with those of cellulose in other solvents as well as of cellulose derivatives and other polysaccharides.

References

1) Kuang, Q.; Zhang, J.; Wang, Z. *J. Phys. Chem. B* **2007,** 111, 9858.

2) Horinaka, J.; Honda, S.; Takigawa, T. *Carbohydr. Polym* **2009,** 78, 576.

3) Kanao, M.; Matsuda, Y,; Sato, T. *Macromolecules* **2003,** 36, 2093-2102.

4) Kasabo, F.; Kanematsu, T.; Nakagawa, T.; Sato, T.; Teramoto, A. *Macromolecules* **2000,** 33, 2748.

5) Yamakawa, H.; Fujii, M. *Macromolecules* **1973,** 6, 407.

6) Yamakawa, H.; Fujii, M. *Macromolecules* **1974,** 7, 128.

7) Yamakawa, H.; Yoshizaki, T. *Macromolecules* **1979,** 12, 32.

8) Yamakawa, H.; Yoshizaki, T. *Macromolecules* **1980,** 13, 633.

9) Yamakawa, H.; Stockmayer, W. H. *J. Chem. Phys* **1972,** 57, 2843.

10) Yamakawa, H.; Shimada, J. *J. Chem. Phys* **1985,** 83, 2607.

11) Shimada, J.; Yamakawa, H. *J. Chem. Phys* **1986,** 85, 591.

12) Henley, D. *Ark. Kemi* **1961,** 18, 327.

13) Saalwächter, K.; Burchard, W. *Macromolecules* **2001,** 34, 5587.

14) Cai, J.; Liu, Y.; Zhang, L. *J. Polym. Sci. B* **2006,** 44, 3093.

15) Yanagisawa, M.; Isogai, A. *Biomacromolecules* **2005,** 6, 1258.

16) Laivins, G. V.; Gray, D. G. *Macromolecules* **1985,** 18, 1746.

17) Aden, M. A.; Bianchi, E.; Ciferri, A.; Conio, G.; Tealdi, A. *Macromolecules* **1984,** 17, 2010.

18) Dayan, S.; Maissa, P.; Vellutini, M. J.; Sixou, P. *Polymer* **1982,** 23, 800.

19) Goebel, K. D.; Harvie, C. E.; Brant, D. A. *Appl. Polym. Symp.* **1976,** 28, 671.

20) Yanai, H.; Sato, T. *Polym. J.* **2006,** 38, 226.

21) Kato, T.; Katsuki, T.; Takahashi, A. *Macromolecules* **1984,** 17, 1726.

22) Nakanishi, Y.; Norisuye, T.; Teramoto, A.; Kitamura, S. *Macromolecules* **1993,** 26, 4220.

23) Norisuye, T. *Polym. J.* **1994,** 26, 1303

24) Ochiai, T.; Terao, K.; Nakamura, Y.; Yoshikawa, C.; Sato, T. *Polymer* **2012,** 53, 3946.

25) Okuyama, K.; Obata, Y.; Noguchi, K.; Kusaka, T.; Ito, Y.; Ohno, S. *Biopolymers* **1996,** 38, 557.

26) Brown, W.; Wikström, R. *Eur. Polym. J.* **1965,** 1, 1.

27) Hirano, I.; Einaga, Y.; Fujita, H. *Polym. J.* **1979,** 11, 901.

28) Nakata, M.; Kawaguchi, T.; Kodama, Y.; Kanno, A. *Polymer* **1998,** 39, 1475.

Appendix. Analysis of the Intrinsic Viscosity of Cellulose in Cadoxen by the Wormlike Chain Model

Henley and Brown and Wikstrom studied the molecular weight dependence of the intrinsic viscosity [η] for cellulose in cadoxen[12, 26)]. Here, cadoxne is a good solvent for cellulose. Figure IIA-1 shows their experimental results by squares and triangles, where M_w is the weight average molecular weight.

The molecular weight dependence of [η] can be also used to determine the wormlike cylinder parameters, the persistence length q, the diameter d, and the excluded volume strength B by fitting to the theory of Yamakawa et al.[5-11)] on [η] for the wormlike cylinder model. The excluded volume effect is not important in lower M region, while the theory is not sensitive to d in higher M region. Therefore, at first values of q and d are suitably chosen to fit to the triangles on the assumption of $B = 0$ (the dotted curve in the Figure), and then the fitting is accomplished by choosing a suitable B value to fit over the whole M region (the solid curve). In this fitting method, the three wormlike cylinder parameters are determined almost uniquely as listed in the figure.

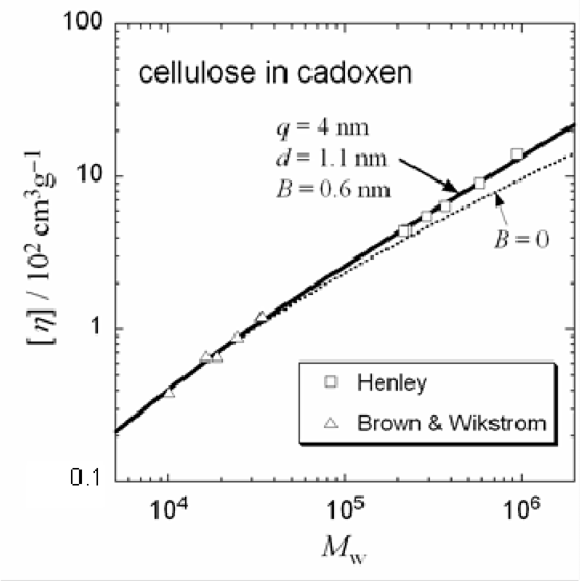

Figure IIA-1. Molecular weight dependence of the intrinsic viscosity [η] for cellulose in cadoxen.

Chapter III. Rheo-Optical Study on Cellulose in Ionic Liquids

III-1. Introduction

Rheological properties of cellulose solutions have been studied for many years using ionic liquids and other solvents.[1, 8-10) However, the interrelation between the dynamic and static segment sizes of the cellulose chain has not been clarified yet. Here, the dynamic segment size is expressed in terms of the Rouse segment size which governs the polymer dynamics, while the static one is represented by the Kuhn segment length which determines the polymer chain conformation.

To compare the dynamic segment size of cellulose in solution with the static one mentioned in Chapter II, EmimMP was selected as a solvent in this chapter. Unfortunately, the glass transition temperature, $T_{g,}$ of EmimMP (−86 °C) is too low to perform the measurements, because rheo-optical measurements can be made only up to the temperature as low as −70 °C. BmimCl makes it possible to perform the rheo-optical measurements near T_g and also over a wider concentration range, because BmimCl has higher T_g and viscosity than EmimMP. For this reason, rheo-optical measurements were also carried out for BmimCl solutions of cellulose in order to discuss the concentration dependence of the dynamic segment size.

Viscoelasticity and birefringence under oscillatory shear flow were measured simultaneously for the solutions of cellulose in EmimMP and BmimCl over a wide range of frequency from the flow to the glassy zone, in order to estimate the Rouse segment size of the cellulose chain in the ionic liquids. The estimated Rouse segment size in EmimMP was compared with the Kuhn segment size of cellulose determined previously from light scattering measurements to discuss the effect of chain rigidity on the relation between the dynamic and static segment sizes of polymer chains in solution.

III-2. Experimental

Materials and Preparation of Solutions. Cotton linter cellulose (CC) in fiber form was supplied from Asahi Kasei Medical Co., Ltd. This is the sample CC1 used in light scattering study mentioned in Chapter II. The weight-average molecular weight, M_w, of the sample was estimated to be 1.40×10^5 in EmimMP and EmimDMP by light scattering (see Chapter II). As the solvent, 1-butyl-3-methylimidazolium Chloride (BmimCl, WAKO) was mainly used without further purification. The CC sample and BmimCl were separately dried in a vacuum oven at 80 °C overnight. The dried sample was dissolved into liquid BmimCl in a vacuum oven at 100˚C for 48 h to prepare the test solutions with the concentrations of 2 and 10 wt%. The powder form was not so effective to improve the dissolution rate of cellulose than the fiber form. All the solutions appeared transparent, stable, and homogeneous when cooled to room temperature. The 2 wt % solution was colorless and the 10 wt % solution was slightly amber.

EmimMP was also used as a solvent of cellulose for the rheo-optical measurement, which was used for light scattering measurements described in Chapter II. CC was dissolved in EmimMP at 1 wt% with same procedure described in Chapter II.

The degradation of cellulose by heating during the dissolution process in ionic liquids has been reported.[10, 11)] The degradation certainly occurred during the dissolution process in both BmimCl and EmimMP. The estimated molecular weight of CC differed between in BmimCl and EmimMP, as mentioned in detail later. I estimated the segment size by data fitting with the Rouse-Zimm model as will be explained later. The effect of degradation during the dissolution process can be corrected by regarding the molar mass as the fitting parameter. The objective of the present study is to estimate the Rouse segment size, which is essentially insensitive to the molecular weight. When the dissolution time was not sufficient, the viscoelastic data varied with time during the measurements at high temperature. Therefore, I chose the dissolution condition at which the good reproducibile data were obtained. I found that further dissolution process (t > 48h) did not affect the viscoelastic data. In addition, for thus prepared samples, the measurements at relatively high temperatures were able to be avoided.

The polymer mass concentration c was calculated from the polymer weight fraction w using the solution density $\rho = 1 \Big/ \left[(1-w)\rho_{\rm S}^{-1} + w\bar{\upsilon} \right]$ with the BmimCl density $\rho_{\rm s}$ = 1.08 g/cm^3 12) and the partial specific volume of cellulose $\bar{\upsilon}$ = 0.50 cm^3/g 6).

Measurements. The viscoelastic measurements were carried out on the solvent, BmimCl, and the CC solutions by ARES G2 (TA Instruments) at various temperatures to obtain the viscoelastic spectra ranging from the flow to the glassy zone with a home-made parallel plate fixture having 4 mm diameter. Instrument compliance was carefully corrected with the method reported by McKenna et al.13, 14) All measurements were performed with small strains in the linear regime. Data obtained at different temperatures were reduced to those at a reference temperature, –25 ˚C, by the method of reduced variables (frequency-temperature superposition) 15).

Simultaneous measurements of stress and flow birefringence under oscillatory shear flow were performed on the solvent and CC solutions with a custom-built rheo-optical apparatus. The details of this apparatus were reported elsewhere.16-18) The He-Ne LASER (λ= 633 nm) was used for the light source. The complex shear modulus, $G^* = G' + \mathrm{i}G''$, and the complex strain-optical coefficient, $K^* = K' + \mathrm{i}K''$, defined as the complex ratio of the shear birefringence component, $n_{\rm xy}$, of refractive index tensor to strain, were determined. The stress-optical rule, SOR, formulated for K^* and G^* is expressed as 19)

$$K' = C\,G' \qquad \text{(III-1)}$$

$$K'' = C\,G'' \qquad \text{(III-2)}$$

Here, proportionality coefficient, C, is the stress-optical coefficient, which can be related with anisotropy of polarizability of segment.

All measurements were performed in the linear viscoelasticity regime at various temperatures. The reliability of the complex moduli was checked by the ARES G2 system. Refractive index of cellulose and BmimCl are, respectively, 1.56 and 1.551 [20)] at 293K, and therefore the form birefringence, which is proportional to the difference of refractive index between polymer and solvent, can be ignored. The glass transition temperature (T_g) and melting point (T_m) were 230 and 339 K, respectively, for BmimCl. [20)]

All measurements were conducted on solutions under the nitrogen atmosphere or dried air to avoid the moisture adsorption of the ionic liquid. Temperature range of measurements was 328~208 K.

III-3. Results and Discussion

III-3-1. Viscoelasticity and Birefringence of BmimCl

Figure III-1 shows the frequency dependence of the complex modulus, G^*, for the neat ionic liquid BmimCl. Here, the method of reduced variables was used to obtain the composite curves in a wide range of frequencies covering to the glassy zone. In the glassy zone, the limiting value of G' is close to 10^9 Pa, and then G^* relaxes monotonically with decreasing frequency, and shows terminal flow behavior characterized by the relationship, $G' \propto \omega^2$ and $G'' \propto \omega^1$. The zero shear viscosity of the solvent, η_0, can be obtained to be ca. 10^5 Pa s at –25 °C by this spectrum. It should be noted that G^* data did not depend on the time after BmimCl was quenched to temperatures close to the glass transition temperature, $T_g = -45$ °C, indicating that the aging effect of BmimCl did not appear within this measurement time scale.

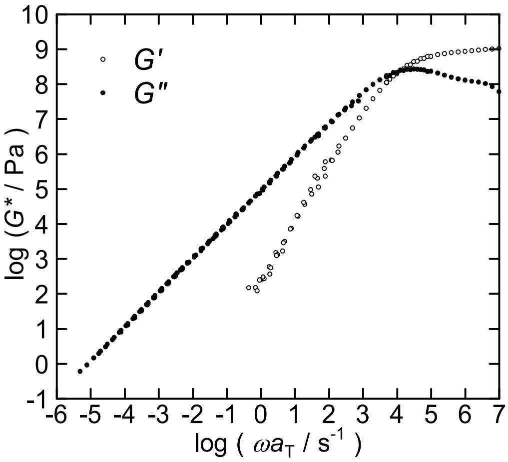

Figure III-1. Frequency dependence of G^* for BmimCl. Reference temperature, T_r, is –25 °C.

Figure III-2 compares the frequency dependence of the strain-optical coefficient, $K^* = K' + iK''$, with that of G^* for BmimCl at –25 °C. The proportionalities hold well between G' and K' and between G'' and K''. However, the proportionality coefficients for the real and imaginary parts are not identical so that the stress-optical rule (SOR) does not hold valid for BmimCl. The SOR has been tested for polymeric liquids and its validity is well established. On the other hand, validity of SOR for low mass glass forming materials has not been examined yet as far as we know. However, it is noted that the proportionality between the stress and the birefringence in the stress relaxation process is not limited to rubbery materials. Assuming that the stress and dielectric tensors are functions of strain, the proportionality just from a symmetry argument under small strains found to be irrespective of the origin(s) of stress21). The breakdown of SOR indicates that the relaxations of stress and birefringence in BmimCl occur with different relaxation times. Kuang et al. suggested that the BmimCl should be considered as a "structured liquid" rather than simple liquid because BmimCl molecules tend to form dynamic clusters[20]. This cluster formation may affect stress and birefringence in different ways.

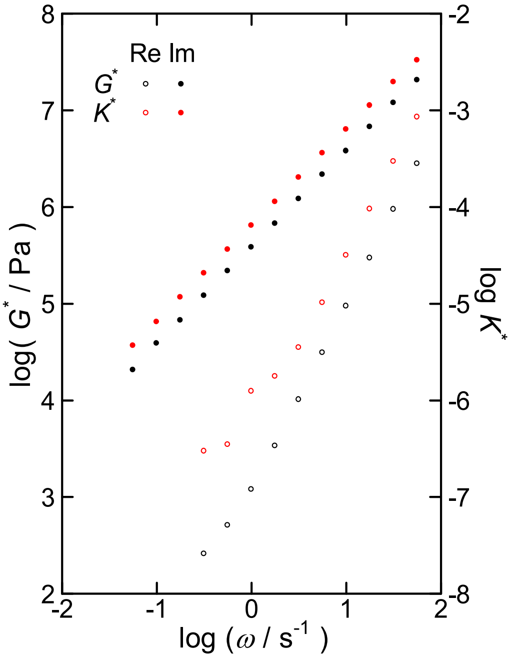

Figure III-2. Frequency dependence of G^* and $K^*$of BmimCl at –25°C.

Figure III-3 shows the temperature dependence of the proportional coefficient C_s between G'' and K'' for BmimCl. This temperature dependence may be related to the strong temperature dependence of correlation length in BmimCl report by Kuang et al.[20] who made dynamic light scattering measurements, and suggested that the cluster structure in BmimCl might change with temperature. In what follows, I refer C_s defined as the ratio of K'' and G'' to as the stress-optical coefficient of the solvent.

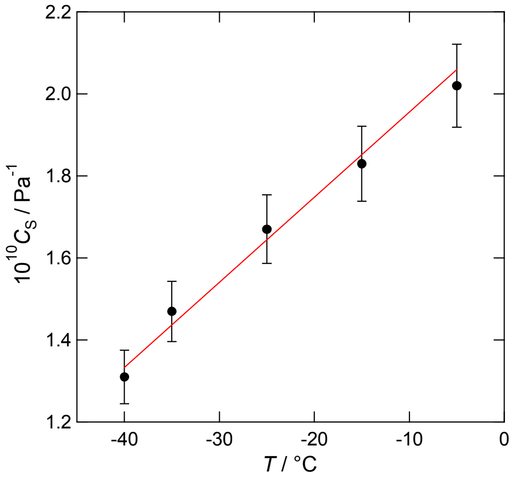

Figure III-3. Temperature dependence of stress-optical coefficient C_s of BmimCl.

III-3-2. Overview of Viscoelasticity and Flow Birefringence of CC Solutions

Figure III-4 shows frequency dependence of the complex modulus G^* and the complex strain-optical coefficient K^* for a BmimCl solution of the cotton linter cellulose (CC) sample with a concentration of 2 wt% ($c = 0.0218\mathrm{gcm}^{-3}$). As I have shown earlier, K^* of neat BmimCl is not themorheologically simple, and therefore only data at –5 °C (squares) and –25 °C (circles) are shown for the clear presentation. I used the same shift factor, a_T, to construct the composite curves for G^* and K^*. It is worthwhile to note that this is the first result of G^* for cellulose solutions observed from the glassy zone to the flow zone. I note that the superposition of K^* at high frequencies, log (ωa_T/s^{-1}) > 0 is not good and systematic deviation is observed. This comes from that the thermo-rheological complexity of K^* as described earlier for neat BmimCl. In the glassy zone, G^* is almost identical with that of pure BmimCl, and the polymer contribution to G^* becomes significant at lower frequencies. The characteristic relationship, $G' \propto \omega^2$ and $G'' \propto \omega^1$, in the terminal flow zone appears only at log (ωa_T/s^{-1}) $\lesssim -2$. Since the polymer contribution to K' is more significant than that to G', the composite curve for K' has a plateau in the intermediate frequency region, which enables us to estimate the Rouse segment size from K' more accurately as described latter.

The viscosity of 2 wt% solution at –25 °C was 2.5×10^5 Pa s, and the intrinsic viscosity, $[\eta]$, was very roughly estimated at 70 $\mathrm{g}^{-1}\mathrm{cm}^3$ from $\eta = \eta_0(1 + [\eta]c + k'[\eta]^2c^2)$ with a typical value of k'=0.5. The coil overlapping concentration, $c^*=2.5/[\eta]$, would be 0.036 g cm^{-3}. Thus, the 2 wt% solution is a dilute solution close to the overlapping concentration.

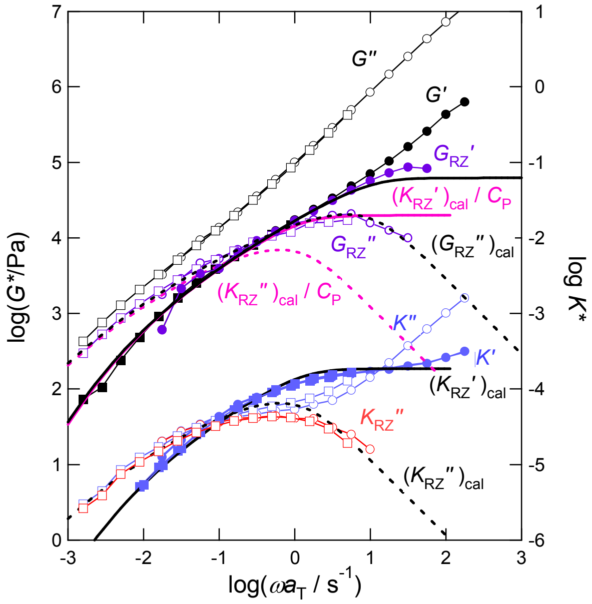

Figure III-4. Frequency dependence of G^* (G', ●, ■; G'', ○, □), K^* (K', ●, ■; K'', ○, □), as well as $G_{\mathrm{RZ}}{}^*$ (G_{RZ}', ●, ■; G_{RZ}'', ○, □) and $K_{\mathrm{RZ}}{}^*$ (K_{RZ}', ●, ■; K_{RZ}'', ○, □) calculated with eqs. III-7 and III-8, respectively, for CC/BmimCl solution at 2 wt%. Reference temperature, T_{r}, is –25 °C. For clear presentation, only data at –5 °C (squares) and –25 °C (circles) are shown. Thick black solid and dashed curves represent values of the Rouse-Zimm theory fitted to $G_{\mathrm{RZ}}{}^*$ and $K_{\mathrm{RZ}}{}^*$, and pink solid and dashed curves indicate theoretical $K_{\mathrm{RZ}}{}^*$ divided by C_{p}.

III-3-3. Estimation of the Cellulose Contribution.

For both of viscoelastic and birefringence measurements, the response of a solution is taken as the sum of polymer and solvating environment contributions (the subscripts p and e denote polymer and environmental contributions, respectively). 22)

$$G^* = G_P^* + G_e^* \tag{III-3}$$

$$K^* = K_P^* + K_e^* \tag{III-4}$$

From several theoretical treatments, viscoelastic (VE) and oscillatory flow birefringence (OFB) properties of dilute solution are predicted to have contributions from long-range (global) and local polymer motions, as well as from chain volume (VE only) and the solvating environment; i.e., four different contributions to VE and three to OFB have been experimentally separated by their different concentration and temperature dependencies.23, 24) Thus, at finite concentrations it is expected

$$G^* = G_{RZ}^* + (G_P^*)_L + (G_P^*)_E + G_e^* \tag{III-5}$$

$$K^* = K_{RZ}^* + (K_P^*)_L + K_e^* \tag{III-6}$$

where the subscript RZ refers to contributions from the global motions (Rouse-Zimm modes), L to those from local motions, E to the Einsteinian contribution, and e to that of the solvating environment. This notation reflects that associated with the discrete helical wormlike chain model of Yoshizaki and Yamakawa 23) and Nagasaka et al. 24)

In earlier studies, 22) experimental results indicated that $(G_P^*)_L + (G_P^*)_E + G_e^*$ and $(K_P^*)_L + K_e^*$ were purely viscous, over the frequency range covered. (Note that the measurements were performed at relatively high temperatures from the glass transition temperature of the solvent by using specially designed high frequency apparatuses.) Therefore, the global motion contribution to the complex modulus, $G_{\mathrm{RZ}}*$, can be experimentally obtained by

$$G_{\mathrm{RZ}}* = G* - \mathrm{i}\,\eta_{\mathrm{S}}(\infty,T)\omega. \qquad \text{(III-7)}$$

Here, $\eta_{\mathrm{S}}(\infty, T) = [(G_{\mathrm{P}}'')_{\mathrm{L}} + (G_{\mathrm{P}}'')_{\mathrm{E}} + G_{\mathrm{e}}'']/\omega$ is the limiting viscosity at high frequencies at temperature, T. Since $G*$ is thermo-rheologically simple, $\eta_{\mathrm{S}}(\infty, T)$ may be written as $\eta_{\mathrm{S}}(\infty)a_{\mathrm{T}} \equiv \eta_{\mathrm{S}}(\infty, T_{\mathrm{ref}})a_{\mathrm{T}}$. Similarly, $K_{\mathrm{RZ}}*$ can be obtained by

$$K_{\mathrm{RZ}}* = K* - \mathrm{i}S_{\mathrm{S}}(\infty,T)\omega \qquad \text{(III-8)}$$

with $S_{\mathrm{S}}(\infty,T) = [(K_{\mathrm{P}}'')_{\mathrm{L}} + K_{\mathrm{e}}'']/\omega$. $S_{\mathrm{S}}(\infty,T)$ may be written as $S_{\mathrm{S}}(\infty)a_{\mathrm{T}} \equiv C_{\mathrm{S}}(T)\,\eta_{\mathrm{S}}(\infty)a_{\mathrm{T}}$.

As shown in Figure III-4, non-zero G' values at high frequencies indicates that the solvating environment contribution, $G_{\mathrm{e}}*$, is not purely viscous as regarded in the earlier studies. However, here the traditional method was firstly examined to estimate the polymer contribution. I estimated $\eta_{\mathrm{S}}(\infty,T)$ and $S_{\mathrm{S}}(\infty,T)$ from the limiting behavior of $G*$ and $K*$ at high frequencies, where contribution of $G_{\mathrm{RZ}}*$ can be ignored. Thus obtained polymer contributions to G'' and K'', G_{RZ}'' and K_{RZ}'', calculated by $G'' - \omega\eta_{\mathrm{S}}(\infty)a_{\mathrm{T}}$ and $K'' - \omega\, C_{\mathrm{S}}(T)\,\eta_{\mathrm{S}}(\infty)a_{\mathrm{T}}$, respectively, are shown in Figure III-4.

It should be noted that at low frequencies, proportionality holds well between K_{RZ}'' and G_{RZ}'', and also between K' and G' with the same proportionality coefficient. The ratio, $K'/G' = K_{\mathrm{RZ}}''/G_{\mathrm{RZ}}''$, corresponding to the stress-optical coefficient for polymer component, C_{RZ}, was obtained as 1.0×10^{-8} Pa^{-1}. This C_{RZ} value was almost 100 times larger than C_s, indicating smaller contribution of solvent component on flow birefringence as described earlier. At high frequencies, the steep increase of G' indicates the significant contribution of other modes including solvating environment. The method to subtract these contributions from G' will be discussed later.

At higher concentration of 10 wt% (c = 0.113gcm^{-3}), the solvent dynamics is significantly modified by the presence of polymer chain. Figure III-5 shows G^* and K^* for the CC/BmimCl solution at the polymer concentration of 10 wt%. The result is similar to those for 2 wt% solution. However, a careful comparison of Figures III-1 and III-5 shows that G^* for 10wt% solution deviates from G^* for neat BmimCl at the high frequency range of log (ωa_T/s^{-1}) <3 in Figure III-5. In addition, the location of G^* and K^* data for 10 wt% solution shift to lower frequencies about one decade. These results clearly indicate that the presence of polymer chain modifies the solvent dynamics as discussed by Lodge.[25)] This means that the polymer contribution cannot be obtained by subtracting the neat “viscous” solvating environmental contribution. I need to find the method to subtract the modified solvent contribution. At high frequency range of $-1 < \log (\omega a_T/\mathrm{s}^{-1}) < 1$, G' and G'' can be described with power laws of ω. Consequently, the RZ term may be obtained by subtracting the modified solvent contribution.

$$G_{RZ}^* = G^* - k_G(\infty,T)\omega^{\alpha} - \mathrm{i}\eta_S(\infty,T)\omega^{\beta} \qquad \text{(III-9)}$$

$$K_{RZ}^* = K^* - k_K(\infty,T)\ \omega^{\alpha} - \mathrm{i}S_S(\infty,T)\omega^{\beta} \qquad \text{(III-10)}$$

With eqs. III-9 and III-10, I obtained apparently reasonable G_{RZ}^*. The results are shown in Figure III-5. Here, I used $\alpha = 0.93$ and $\beta = 0.87$.

Eq. III-9 was also used for estimating G_{RZ}' for the 2 wt% solution. (α= 1.5 was determined in the frequency range of $1 < \log(\omega a_T/s^{-1}) < 3$ of Figure III-1).

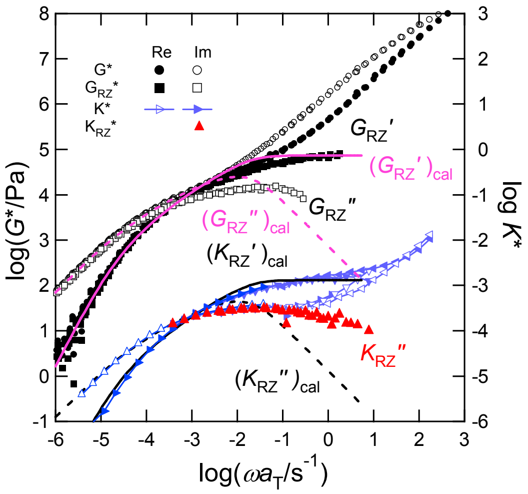

Figure III-5. Frequency dependence of G^* (G', ●; G'', ○) measured by ARES-G2 and RZ term G_{RZ}^* (G_{RZ}', ■; G_{RZ}'', □), for a CC/BmimCl solution of 10 wt%. Also included are K^* (light blue unfilled and filled triangles, 15 °C(up), –5 °C(right), –15 °C(down), and –25 °C(left)) and K_{RZ}''(▲). Reference temperature, T_r, is –25 °C. Thick solid and dashed curves represent values of the Rouse-Zimm theory for G_{RZ}^*(pink) and K_{RZ}^* (black).

A comment may be needed for the above analysis using power laws for the modified solvent dynamics. The phenomenological theory requires that the exponent of the power law should have the relaxation $\alpha = \beta$ and $\tan\delta = \tan(\pi\alpha/2)$. This type of power law has been used to define the critical point of gels. It is noted that the power law with $\alpha \neq \beta$ holds only in the limited frequency region. In addition, extrapolation of power law with $\alpha < 2$ and $\beta < 1$ to low frequencies causes a problem because the modified solvent contribution overcomes the RZ term which shows the terminal flow behavior $G' \propto \omega^2$ and $G'' \propto \omega^1$ at low frequencies. Hence, the power law for the modified solvent dynamics contradicts to the terminal flow behavior of the

RZ term. The power law must have a cut off frequencies to obey the terminal flow behavior at low frequencies.

An alternative method to estimate G_{RZ}* is to use the modified stress-optical rule, which is based on the SOR for each contributions. [26, 27] The rule can be written as follows.

$$G^* = G_{RZ}^* + G_G^* \tag{III-11}$$

$$K^* = K_{RZ}^* + K_G^* = C_{RZ}G_{RZ}^* + C_G G_G^* \tag{III-12}$$

The G_G* and K_G* terms represent the glassy responses of solution which include all contributions of the local motion of polymer, the Einsteinian contribution, and the solvating environment. Thus, molecular origin of the G_G* and K_G* terms is somehow complex. However, I found that the SOR held well experimentally between G_G* and K_G* for 10 wt% solution, even though the SOR did not hold strictly for neat BmimCl. The breakdown of SOR for BmimCl is a subtle issue as shown in Figure III-2 and therefore broadening of the relaxation spectra at high concentrations increases the similarity of the mechanical and optical relaxation spectra, resulting in apparent establishment of SOR for the glassy response. I found that the proportionality coefficient, C_G, determined experimentally depended on temperature, reflecting temperature dependence of C_S. Since the values of C_{RZ} and C_G can be determined experimentally, eqs. III-11 and III-12 can be regarded as a simultaneous equations for G_{RZ}* and G_G*. The G_{RZ}* and G_G* components determined by solving eqs. III-11 and III-12 are shown in Figure III-6. A comparison of Figure III-5 and 6 reveals that the G_{RZ}* obtained by the two methods are consistent with each other, at the frequency range of $-4 < \log (\omega a_T/s^{-1}) < 3$.

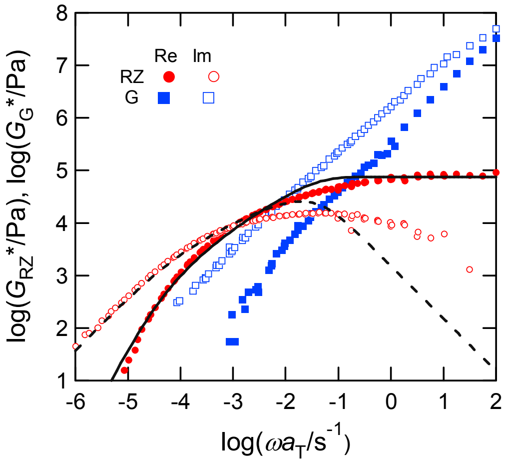

Figure III-6. Rouse-Zimm and glassy contributions of G^* for a CC/BmimCl solution of 10 wt%, indicated by red and blue symbols, respectively. Reference temperature, T_r, is –25 °C. Lines represent Rouse-Zimm theoretical curves for G_{RZ}^*.

Figure III-7 shows the frequency dependence of G^* for an EmimMP solution of the cellulose sample CC, measured by ARES-G2 and K^* as well as K_{RZ}''. Even at 1 wt%, G^* showed the rubbery plateau region indicating chain entanglements in this system. This result indicates that the molecular weight of CC is larger in EmimMP than that in BmimCl. This difference might come from less degradation of the cellulose chain in EmimMP than in BmimCl, because of the lower dissolution temperature at the dissolution of cellulose in EmimMP.

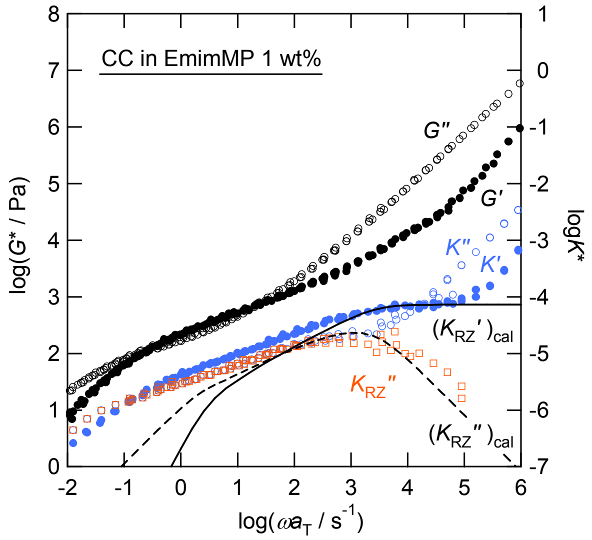

Figure III-7. Frequency dependences of G^* (G', ●; G'', ○) measured by ARES-G2 (filled and unfilled circles) and of K^* (K', ●; K'', ○) as well as K_{RZ}'' (□). Reference temperature, T_{r}, is –25 °C. Lines represent Rouse-Zimm theoretical curve, K_{RZ}*.

III-3-4. The Rouse segment size of cellulose in Ionic Liquids

According to the Rouse-Zimm theory [28, 29] based on the bead-spring model, the polymer contribution of the linear polymer solution with the polymer mass concentration, c, is given by

$$\left(G_{RZ}^{*}(\omega)\right)_{cal} = \frac{cRT}{M}\sum_{i=1}^{N}\frac{i\omega\tau_P}{1+i\omega\tau_P} \tag{III-13}$$

$$\tau_P = \frac{\tau_{RZ}}{p^k} \quad (1.5 \le k \le 2) \tag{III-14}$$

Here, RT is the gas constant multiplied by the absolute temperature, M and N are the molar mass and number of segments per chain of the polymer, respectively, and τ_{RZ} is the longest relaxation time of the bead-spring model. The value of k in the Rouse-Zimm model indicates the transition from the free-draining limit (k =2.0) to the non-free-draining limit (k =1.5). For natural polymers, molar mass distribution should be considered. If the molar mass distribution is considered, eqs III-13 and III-14 are modified as follows. [30)]

$$\left(G_{RZ}^{*}(\omega)\right)_{cal} = \sum_{M=0}^{\infty} x_M \frac{cRT}{M} \sum_{i=1}^{N} \frac{i\omega\tau_P}{1+i\omega\tau_P} \tag{III-15}$$

$$\tau_{\mathrm{p}} = \frac{\tau_{\mathrm{R}}}{p^k} M^k \tag{III-16}$$

Here, x_{M} is the number fraction of polymers with the molar mass, M. I have no information of molar mass distribution. However, if the chain breakage statistically occurred by the degradation during the dissolution process, the molar mass distribution should follow the most probable distribution. In that case of the most probable distribution, x_{M} is represented by eq III-17, where M_{n} and M_{w} are the number- and weight-average molecular weights, respectively.

$$x_{\mathrm{M}} = \frac{1}{M_{\mathrm{n}}} \exp\left(-\frac{M}{M_{\mathrm{n}}}\right) = \frac{2}{M_{\mathrm{w}}} \exp\left(-\frac{2M}{M_{\mathrm{w}}}\right) \tag{III-17}$$

Black solid and dashed curves for G' and G'', respectively, in Figure III-4 indicate theoretical values calculated by eqs III-15 – III-17. Molar mass can be obtained through data fitting with eqs III-15 – III-17, without of the absolute M_{w} value, if molar mass is regarded as the fitting parameter. In the infinite dilute regime, thus determined M_{w} value corresponds to the true M_{w} value, $M_{\mathrm{w}}^{\mathrm{true}}$. However, at the finite concentration regime, G^* is modified by the molecular interaction. The effect of inter-chain interaction on viscoelastic spectra around the coil overlapping concentration, c^*, has been studied by Osaki *et al.* for mono-disperse molar mass distribution system [31)] and later by Morishima and Inoue for polydisperse systems[32)]. For the mono-disperse systems, Osaki *et al.* clarified that the slow mode is needed in addition to the RZ terms to reproduce the experimental data and that the magnitude of the slow mode increases with increasing of c/c^*. At higher concentrations, the slow mode grows up to the entanglement plateau modulus. Fitting with eqs. III-15 – III-17 still works apparently well around c^* for the case of most probable distribution, but the obtained molar mass, M_w^{app}, increases with increasing concentration. The ratio, M_w^{app} / M_w^{true} can be described by a universal function of c/c^*.[32)]

I have chosen the number averaged molecular mass, M_w^{app}, of CC to be 40,000 to obtain a good fitting of the low frequency region data with $k = 2$ corresponding to Rouse model. This exponent may be natural because the concentration is close to c^* and therefore the hydrodynamic interactions would be screened out. For 2 wt% solution being close to c^*, the corrected M_w^{true} value would be expected as 28,000.[32)] This value is considerably smaller than $M_w = 1.4\times10^5$ obtained by light scattering in EmimMP and EmimDMP, indicating the M_w loss in BmimCl would occur in dissolution process at 100°C. The good data fitting with the small M_w suggest that self assembly of the cellulose chains in BmimCl would not occur.

Similarly, for the 10 wt% solution, larger M_w^{app} value, 1.0×10^5 was needed for the best data fitting due to the stronger inter-chain interaction. The M_w^{true} value was obtained as 25,000 by correcting the effect of finite concentration. The theoretical fitting for G_{RZ}^* in the moderate frequency region is not very good at 10 %. This ill fit can be attributed to the concentration fluctuation, which causes the distribution of monomeric friction coefficient. The molar mass between the entanglements, M_e, for a hypothetical molten state of cellulose is reported to be 3500 g mol^{-1} so that M_e for 10wt% solution is predicted to be 35000 g mol^{-1},[5)] which is comparable to the molar mass of our cellulose sample. This estimation clearly indicates that 10 wt% solution is a non-entangled system and why the rubbery plateau region is not observed in G^*.

The Rouse segment size can be automatically estimated by fitting the data of G_{RZ}^*. However, for 10 wt% solution, data fitting with the Rouse-Zimm theory was not satisfactory for G'' at high frequencies. This can be attributed to the concentration fluctuation as described earlier. The limiting modulus at high frequencies, $G'_{RZ}(\infty)$, can be obtained more easily and precisely. The value of $G'_{RZ}(\infty)$ was 6.3×10^4 Pa at 2 wt% and 8.5×10^4 Pa at 10 wt% and the molar mass of the Rouse segment size, M_s, was estimated as ca. 700 g mol^{-1} at 2 wt% and 2300 g mol^{-1} at 10 wt% by following equation.[33)]

$$M_S = \frac{cRT}{G_{RZ}'(\infty)} \qquad \text{(III-18)}$$

Using SOR, the Rouse-Zimm theory can be also applied to K_P^*, which is calculated by $C_P G_P^*$ with the stress-optical coefficient C_P and eqs III-1 and III-2. Solid and dashed curves for K^* in Figures III-4 – III-6 are the fitting results. From SOR, M_s was estimated by eq III-19 as follows.

$$M_S = \frac{C_P cRT}{K_{RZ}'(\infty)} \qquad \text{(III-19)}$$

The obtained value of M_s was 2300 g mol^{-1} for both 2 and 10 wt%, about 3 times larger than that of estimation with viscoelastic data for 2 wt%. Because of smaller solvent contribution to K' than to G', the estimate of $K'_{RZ}(\infty)$ should be more accurate than $G'_{RZ}(\infty)$. However, the difference in M_s obtained from $K'_{RZ}(\infty)$ and $G'_{RZ}(\infty)$ is appreciable, and cannot be explained by experimental errors, because pink solid and dashed curves calculated for G' and G'' by eq III-1, which gives M_s = 2300 g mol^{-1}, appreciably deviate from the experimental data in an intermediate frequency region. I speculate that local modes of cellulose chain smaller than the Rouse segment size might contribute to the modulus. The $(G_P^*)_L$ term in eq III-3 is a candidate for such a mode. (In this context, $\eta_S(\infty)$ corresponds to $(G_P'')_L/\omega$.) For our best knowledge, local modes such as a glassy mode have normally a small stress-optical coefficient, ~ 10^{-11}Pa^{-1}, and consequently its contribution to the birefringence, $(K_P'')_L$ would be difficult to experimentally observe.

In Figure III-7, K_{RZ}'' for the CC/EmimMP solution obtained from eq. III-8 was not able to be described with the Rouse-Zimm theory (the thin dashed curve in the figure) in a lower frequency region. This is because the Rouse-Zimm theory does not include the entanglement effect. However, since the entanglement effect may not be important in a higher frequency region, the fitting by the Rouse-Zimm theory was made at log $(\omega a_T/\mathrm{s}^{-1}) > 2$. The thin dashed curve in Figure III-7 indicates the fitting result, which gives the $K'_{RZ}(\infty)$ value. From this $K'_{RZ}(\infty)$ value, M_s was estimated as 4700 g mol^{-1}. This value is about twice as that in BmimCl estimated above. The difference of M_s depending on solvent spices would be caused by the difference of the mobility of solvent molecules. Viscosity of EmimMP is much lower than that of BmimCl, and therefore the fast mobility of EmimMP molecules made the dynamic rigidity of the cellulose chain higher than that in BmimCl.

III-3-5. Comparison between the Rouse and Kuhn segment sizes

The conformation of linear polymer chains can be characterized in terms of the wormlike chain model, where the *static* segment size of the polymer chain is represented by the persistence length q or the Kuhn statistical segment length $b_K \equiv 2q$. It is well known that cellulose is a typical semiflexible polymer, and its q or b_K has been studied for a long time. As shown in Chapter II, q (b_K) of cellulose in EmimMP and EmimDMP was estimated to be 7 nm (14 nm), which is much larger than q = 1 nm (b_K = 2 nm) of polystyrene in cyclohexane. Similar q values for cellulose were reported in well-known cellulose solvents (see Table II-3).

Recently, Chen et al. made static light scattering measurements on solutions of a cotton cellulose sample dissolved in an ionic liquid, 1-allyl-3-methylimidazorium chloride (AmimCl) and determined the weight average molecular weight and the z-average radius of gyration to be 7.9×10^5 and 75 nm, respectively.6) The analysis of the wormlike chain model provides us 5.5 nm (11 nm) for q (b_K), which is rather close to the result in EmimMP and EmimDMP. The persistence length 7 nm gives the molar mass of the Kuhn segment M_K to be 4400 g mol^{-1}. This value of M_K is almost identical with M_s (= 4700 g mol^{-1}) estimated above from $K_{RZ}'(\infty)$ for CC in EmimMP, and slightly larger than M_s (= 2300 g mol^{-1}) estimated from $K_{RZ}'(\infty)$ in BmimCl. Thus, the relationship $M_s \approx M_K$ holds well for cellulose in solution. A comment may be needed for the present result of $M_s \approx M_K$ in solution. M_s for a typical flexible polymer polystyrene in solution ~5000 g mol^{-1} is known to be ca. five times as large as M_K ~1000 g mol^{-1}while M_s~800 g mol^{-1} in melt. Thus, for the case of polystyrene, M_s strongly depends on concentration. On the other hand, for the case of cellulose, $M_s \approx M_K$ is satisfied even in solution, suggesting that M_s of cellulose would not depend on concentration. The present result implies that the relation between the Rouse and Kuhn segment sizes in solution depends on the chain rigidity.

Larson argued the dynamic segment size of the polymer chain under high-frequency oscillations using the bent rigid wires model.34) He considered a polymer chain consisting of a number of main-chain chemical bonds, of which conformation changes by the internal rotation around each bond. If the internal rotation occurs under the rotational potential with the activation energy ΔE_{a}, the time τ_{b} required for the bond rotation may be expressed by

$$\tau_{\mathrm{b}} = \frac{6\pi\eta_0 b^3}{k_{\mathrm{B}}T}\beta \exp\left(\frac{\Delta E_a}{k_{\mathrm{B}}T}\right) \tag{III-20}$$

where η_0 is the solvent viscosity, b is the bond length, k_{B} is the Boltzmann constant, and β is a dimensionless prefactor that can be estimated from the shape of the rotational potential.

In the Rouse model, on the other hand, each Rouse segment is assumed to behave as a bead with a diameter b_{R}. The Rouse segment size b_{R} may be defined as the size of subchain of which rotational relaxation time $\tau_{\mathrm{r,s}}$ is identical with τ_{b} given by eq III-20. If the Rouse segment consists of $N_{\mathrm{K,s}}$ Kuhn's segments, the rotational relaxation time $\tau_{\mathrm{r,s}}$ of the Rouse segment is given approximately by

$$\tau_{\mathrm{r,s}} = \kappa \frac{\eta_0 {b_{\mathrm{K}}}^3 {N_{\mathrm{K,s}}}^{3/2}}{k_{\mathrm{B}}T} \tag{III-21}$$

where b_{K} is the Kuhn segment length and κ is a proportional constant. In the theories of Rouse and Zimm, κ is taken to be 0.16 and 0.2, respectively, but it should depend on the polymer concentration through the inter-segment hydrodynamic interaction. To obtain eq III-21, the excluded volume effect was ignored, because $N_{\mathrm{K,s}}$ is not a large number. Equality of τ_{b} and $\tau_{\mathrm{r,s}}$ given in eqs III-20 and III-21 provides the following relation

$$N_{\mathrm{K,s}} = \left(\frac{6\pi\beta}{\kappa}\right)^{2/3} \left[\frac{b}{b_{\mathrm{K}}}\exp\left(\frac{\Delta E_{\mathrm{a}}}{3k_{\mathrm{B}}T}\right)\right]^2 \tag{III-22}$$

For polystyrene, values of b, b_{K}, and ΔE_{a} are known to be 0.153 nm, 2 nm, and 14.6 kJ/mol (the energy barrier height between the trans and gauche conformations of *n*-butane), respectively. Using these values and assuming $\beta/\kappa = 3.7$, eq III-22 provides $N_{\mathrm{K,s}} = M_{\mathrm{s}}/M_{\mathrm{K}} = 5$, being in agreement with the experimental result. On the other hand, b and b_{K} for the cellulose chain are 0.55 nm and 14 nm, respectively. The height of the energy barrier ΔE_{a} for the cellulose chain to take the kink conformation, as mentioned in Chapter I, is not known, but it must be higher than the Gibbs energy of the kink conformation $G^* = 4.9$ kJ/mol (see Section I-3-1 in Chapter I). When ΔE_{a} is chosen to be 14 kJ/mol along with $\beta/\kappa = 3.7$, eq III-22 gives $N_{\mathrm{K,s}} = M_{\mathrm{s}}/M_{\mathrm{K}} = 1.1$ (the experimental result obtained in this study). The value of ΔE_{a} chosen is comparable to that for the polystyrene chain.

The estimated value of M_{s} (= 700 g mol^{-1}) from $G_{\mathrm{RZ}}'(\infty)$ for the 2 wt% solution is too small in comparison with M_{K} because the Rouse segment should not be smaller than the Kuhn segment, as mentioned above. As discussed earlier, this too small M_{s} value may be attributed to the presence of local modes besides polymer global motions, which can significantly contribute to only rheological data G^*.

Conclusions

I reported the rheo-optical data for BmimCl which behaved as a glass-forming simple liquid on the viscoelasticity. The SOR did not hold for BmimCl and the ratio of birefringence to the stress depended on temperature. These results suggest the presence of some temperature-dependent structure such as clusters even in the liquid state near the glass transition temperature.

In BmimCl, the molar mass of the Rouse segment size, M_s, estimated by rheological data, 700 g mol^{-1}was much smaller than that by optical data, 2300 g mol^{-1}. This suggests that the additional local mode in addition to chain diffusion appearing mechanical (rheological) data is not observed in optical data. The subtraction of environmental contribution including solvent contribution from birefringence is more accurate because of lower contribution of solvent and local modes to birefringence than to viscoelasticity. The M_s value estimated by optical data for cellulose in EmimMP was 4700 g mol^{-1}, which is slightly larger than that in BmimCl.

The value of the molar mass of the Kuhn segment M_K for cellulose in Chapter II is almost same as our result M_s in the same solvent EmimMP. This relation $M_s \approx M_K$ in solution forms a sharp contrast to the corresponding relation for polystyrene, a flexible polymer: $M_s \approx 5M_K$ in solutions. This result indicates that relation of M_s and M_K depends on the chain stiffness.

References

1) Blachot, J. F.; Brunet, N.; Navard, P.; Cavaille, J. Y. *Rheol. Acta* **1998,** 37, 107.

2) Swatloski, R. P.; Spear, S. K.; Holbrey, J. D.; Rogers, R. D. *J. Am. Chem. Soc.* **2002,** 124, 4974.

3) Remsing, R.; Swatloski, R.; Rogers, R.; Moyna, G. *Chem. Commun.* **2006**, 1271.

4) Kuang, Q.; Zhao, J.; Niu, Y.; Zhang, J.; Wang, Z. *J. Phys. Chem. B.* **2008,** 112, 10234.

5) Horinaka, J.; Yasuda, R.; Takigawa, T. *J. Polym. Sci. B. Polym. Phys* **2011,** 49, 961.

6) Chen, Y.; Zhang, Y. M.; Ke, F. Y.; Zhou, J. H.; Wang, H. P.; Liang, D. H. *Polymer* **2011,** 52, 481.

7) Chen, X.; Zhang, Y.; Wang, H.; Wang, S.-W.; Liang, S.; Colby, R. H. *J. Rheol.* **2011,** 55, 485.

8) Tamai, N.; Tatsumi, D.; Matsumoto, T. *Biomacromolecules* **2004,** 5, 422.

9) Saalwächter, K.; Burchard, W. *Macromolecules* **2001,** 34, 5587.

10) Haward, S. J.; Sharma, V.; Butts, C. P.; McKinley, G. H.; Rahatekar, S. S. *Biomacromolecules* **2012,** 13, 1688.

11) Zhang, H.; Wu, J.; Zhang, J.; He, J. S. *Macromolecules* **2005,** 38, 8272.

12) Horinaka, J.; Honda, S. *Carbohydr. Polym.* **2009,** 78, 576.

13) Hutcheson, S. A.; McKenna, G. B. *J. Chem. Phys.* **2008,** 129, 074502.

14) Schroter, K.; Hutcheson, S. A.; Shi, X.; Mandanici, A.; McKenna, G. B. *J. Chem. Phys.* **2006,** 125, 214507.

15) Ferry, J. D., Chapter 11 Dependence of Viscoelastic Behavior on Temperature and Pressure. In *Viscoelastic Properties of Polymers*, 4th *Ed.* ed.; Wiley: New York, 1980; pp 264.

16) Iwawaki, H.; Inoue, T.; Nakamura, Y. *Macromolecules* **2011,** 44, 5414.

17) Hayashi, C.; Inoue, T. *Nihon Reoroji Gakkaishi* **2009,** 37, 205.

18) Watanabe, H.; Inoue, T. *Materials Science and Engineering a-Structural Materials Properties Microstructure and Processing* **2006,** 442, 361.

19) Janeschitz-Kriegl, H., *Polymer Melt Rheology and Flow Birefringence*, Springer-Verlag: Berlin, 1983; p 524.

20) Kuang, Q.; Zhang, J.; Wang, Z. *J. Phys. Chem. B.* **2007,** 111, 9858.

21) Born, M.; Wolf, E., *Principles of Optics*. 7th ed.; Cambridge University Press: Cambridge, 1999.

22) Peterson, S. C.; Echeverria, I.; Hahn, S. F.; Strand, D. A.; Schrag, J. L. *J. Polym. Sci. Part B: Polym. Phys.* **2001,** 39, 2860.

23) Yoshizaki, T.; Yamakawa, H. *J. Chem. Phys.* **1988,** 88, 1313.

24) Nagasaka, K.; Yoshizaki, T.; Yamakawa, H. *J. Chem. Phys.* **1989,** 90, 5167.

25) Lodge, T. P. *J. Phys. Chem.* **1993,** 97, 1480.

26) Inoue, T.; Okamoto, H.; Osaki, K. *Macromolecules* **1991,** 24, 5670.

27) Inoue, T.; Uematsu, T.; Osaki, K. *Macromolecules* **2002,** 35, 820.

28) Rouse, P. E. *J. Chem. Phys.* **1953,** 21, 1272.

29) Zimm, B. H. *J. Chem. Phys.* **1956,** 24, 269.

30) Sammler, R. L.; Landry, C. J. T.; Woltman, G. R.; Schrag, J. L. *Macromolecules* **1990,** 23, 2388.

31) Osaki, K.; Inoue, T.; Uematsu, T.; Yamashita, Y. *J. Polym. Sci. Part B: Polym. Phys.* **2002,** 40, 1038.

32) Morishima, K.; Inoue, T. *J. Soc. Rheology Jpn.* **2013,** 41, 151.

33) Inoue, T. *Macromolecules* **2006,** 39, 4615.

34) Larson, R. G. *Macromolecules* **2004,** 37, 5110.

35) Flory, P. J., *Statistical Mechanics of Chain Molecules*. John Wiley & Sons: New York, 1969.

Chapter IV. Rheo-Optical Study on Cellulose Derivatives

IV-1. Introduction

In Chapter III, the viscoelasticity and birefringence was investigated for dilute to semi-dilute solutions of cellulose. As mentioned in Chapter I, it is difficult to dissolve cellulose in any solvents up to high concentrations because of its poor solubility. In fact, even in ionic liquids, the solubility limit of cellulose is only about 10 %. In addition, molten cellulose cannot be achieved because of intermolecular hydrogen bonds and therefore direct characterization of molten cellulose has not been performed. Thus, it is difficult to character dynamics of the cellulose chain over a wide concentration region.

Matsumoto and his coworkers found that tunicate cellulose, having poorer solubility than other kinds of cellulose, dissolved in LiCl / 1,3-dimethyl-2-imidazolidinone (DMI). 1)By using DMI, they discussed difference in rheological properties of cellulose solutions from various biological sources. 1,2) According to their results, the concentration dependence of viscosity varies with biological origins and it does not follow a universal scaling relation. However, the rubbery plateau modulus, G_N, for the cellulose solutions does not depend on the biological source and can be summarized as the following equation.

$$G_N/\mathrm{MPa} = 5.49\phi_w^{2.14} \qquad \text{(IV-1)}$$

Here ϕ_w is the weight fraction of cellulose.

The front factor of eq. IV-1 corresponds to G_N for neat cellulose in a hypothetical molten state (cellulose melt). This value G_N^{melt} seems to be somehow too large because it gives the molar mass between entanglements in melt, M_e^{melt} (= $\rho RT / G_N^{\mathrm{melt}}$) ~ 720 g mol^{-1}, using the literature value $\rho = 1550$ kgm^{-3}. This M_e^{melt} corresponds to 4.5 D-glucose units per strand between neighboring entanglement points. On the other hand, light scattering experiments on dilute cellulose solution indicates that cellulose is a stiff chain and the molar mass of the Kuhn segment, M_K, is larger than 4400 g mol^{-1} (see Chapters II and III). Thus, M_e^{melt} value from eq. IV-1 is much smaller than the statistical segment size, suggesting that dynamics of the cellulose chain cannot be treated by the Gaussian chain dynamics.

However, Matsumoto et al. claimed that the value of the front factor of eq. IV-1 is for a "hypothetical" melt, which is created hypothetically from solution merely by increasing the number of the polymer chain in solution, and therefore it may differ from the actual cellulose melt. They also reported that G_N^{melt}/MPa = 2.2 for cellulose in NMMO, and Takigawa et al. reported M_e = 3500 g mol^{-1} for cellulose in BmimCl.5) These results indicate that the front factor of eq. IV-1 depends on solvent species.3) It is noted, however, that the rubbery plateau modulus of polystyrene in solution does not depend on solvent quality including θ-solvent if the volume fraction is the same.4) Thus, the value of M_e for cellulose in melt is still open for question.

In order to speculate rheological properties of the molten cellulose, there is another approach. Yamaguchi et al. reported complex shear modulus of cellulose acetate propionate (CAP) in their study on optical properties of CAP6). While cellulose acetate is a crystalline polymer even if the degree of substitution per glucose units is close to 3, CAP is a non-crystalline polymer. According to their result, G_N of CAP melt is 2×10^5 Pa. This value is order of magnitude smaller than G_N value in eq. IV-1. Although the effect of esterification on the inter-chain interaction and on the chain conformation is not obvious, the ester groups would work as a plasticizer (solvent) and decrease the volume fraction ϕ of the cellulose main chain in bulk. If the effects on the inter-chain interaction and the chain conformation are ignored, one can estimate G_N^{melt} for cellulose as 8.5 × 10^5 Pa, using the generally accepted relation $G_N \sim \phi^2$ and the volume fraction of ester groups of CAP (= 0.485). This G_N^{melt} value is still much smaller than the front factor of eq. IV-1, and the M_e^{melt} value for cellulose melt is estimated to be 4300 g mol^{-1}, which is fairly close to the M_e^{melt} value estimated from cellulose / ionic liquid system (M_e^{melt} =3500 g mol^{-1}).5)

Another method to estimate the M_e^{melt} value for hypothetical cellulose melt is to apply the theories for the entanglement length. Among these theories, concept of the packing length is widely accepted. According to this theory,7,8) the rubbery plateau modulus can be related to molar mass of repeating unit, M_0.

$$G_N^{\ melt} = BT\left(\frac{\langle R^2\rangle \rho}{M}\right)^3 = BTb^6\left(\frac{\rho}{M_0}\right)^3 \qquad \text{(IV-2)}$$

Here, B is a numerical constant and T is the absolute temperature. $\langle R^2 \rangle$, M , and ρ are the mean square of the end to end distance, molar mass of chain, and density, respectively. b is the virtual bond length of the repeating unit. If it is assumed that the chain dimension is not varied with esterification, b becomes constant. For such a case, eq. IV-2 expects M_e^{melt} = 1500 g mol^{-1}, and this value is smaller than the Kuhn segment size. As I will discuss later, and already discussed by Horinaka5), this theory does not work well for cellulose and linear D-glucans, and therefore the relationship between the entanglement size and molecular structure is still open for question.

In this study, I examined the dynamical chain rigidity and M_e^{melt} of cellulose acetate butyrate (CAB) and cellulose acetate propionate (CAP) in melts by simultaneous measurements of dynamic birefringence and viscoelasticity. The relation between M_e^{melt} and M_s is discussed and compared with the reported results for some engineering plastics9) including Bisphenol-A polycarbonate[10)].

IV-2. Experimental

Sample. Commercially available cellulose acetate butyrate, CAB, (Eastman Chemical Company, CAB-321-0.1) and cellulose acetate propionate, CAP, (Eastman Chemical Company, CAP-482-20) was used. Characterizations of CAB and CAP are summarized in Table IV-1.[11,12)] According to the supplier' s data sheet, densities of CAP and CAB are, respectively, 1220 kgm^{-3} and 1200 kgm^{-3}. Powder sample were compressed into a flat sheet with 0.5mm thickness by a compression-molding machine for 5 min at 220°C under 5 MPa.

Method. The simultaneous measurements of dynamic birefringence and viscoelasticity were performed under isothermal condition above the glass transition temperature over a frequency range of 1 – 130 Hz. All measurements were performed in the linear viscoelastic regime. Typical strain amplitude was 0.01% in the glassy zone and 0.2% in the rubbery zone. The Rheometric ARES and TA ARES G2 systems were also used to check the reliability of the complex Young's modulus measurements. The complex shear modulus, G^*, at various temperatures was measured to obtain the viscoelastic spectra ranging from the flow to the glassy zone with a home-made parallel plate fixture with 4 mm diameter. Instrument compliance was carefully corrected with the method reported by McKenna et al.[13,14)] All measurements were performed with small strains in the linear regime. Data obtained at different temperatures were reduced to those at a reference temperature, 150 ˚C, by the method of reduced variables (frequency-temperature superposition) [15)].

Table IV-1. Charactarization of cellulose esters

	Degree of substitution			
Polymer	Acetyl	Propionyl or butyryl	ρ / kg m^{-3}	M_n / 10^4
CAP	0.19	2.58	1220	2.1
CAB	1.06	1.8	1200	1.2

IV. Results and Discussion

IV-3-1. Viscoelasticity and Birefringence of CAB and CAP

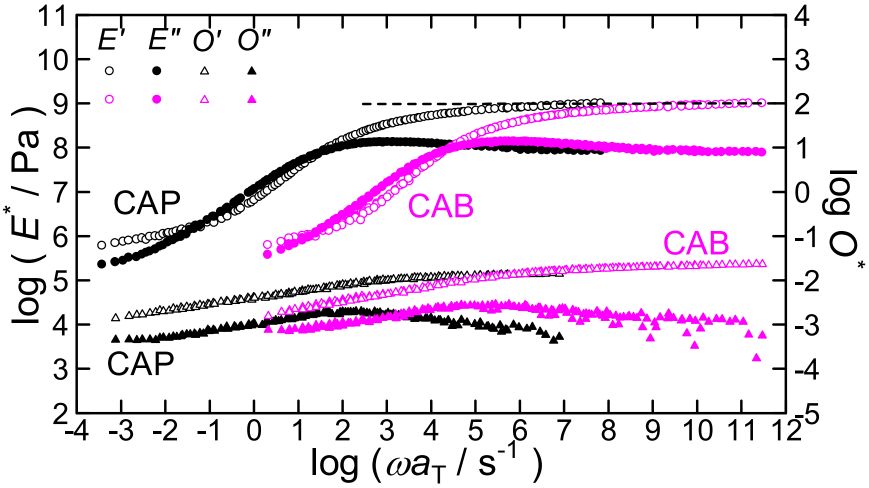

Figure IV-1. Composite curves for complex Young's modulus, complex shear modulus, and complex strain-optical coefficient forCAB and CAP. Reference temperate is 150°C.

Figure IV-1 shows the composite curves of E^* and O^* for CAB. Here, we used the method of reduce variables to construct the composite curves[15)] and the reference temperature is 150°C. The different shift factor a_T was used for E^* and O^* separately. Although failure of the method of reduced variable is often observed around the glass-to-rubber transition,[16,17)] the superposition is fairly well for both the curves.

The agreement of E^* and $3G^*$, measured different system each other, is quite well over the whole frequency region, and therefore the reliability of E^* is confirmed.

The limiting value of modulus at high frequencies, the glassy modulus, is slightly lower than that for polystyrene, 17) but close to that for bisphenol-A polycarbonate, PC10). Since the relationship between the height of the glassy modulus and molecular structure is not well established, further discussion on the height of the glassy modulus is out of scope of the present study.

At low frequencies, the ω dependence of the modulus for CAB is weak and the rubbery plateau modulus, G_N, could be estimated to be $E_N/\mathrm{Pa} = 3G_N/\mathrm{Pa} = 7.9 \times 10^5$. Here, the G_N value was determined as the G' value at the inflection point of the graph of log G' versus log ω.18) If I assume that the ester groups work as a plasticized as explained earlier, G_N for cellulose melts is estimated as 1×10^6 Pa from the concentration dependence of the rubbery plateau modulus, $G_N \sim \phi^2$, where ϕ is the concentration of polymer.

The frequency dependence of O^* is weak and similar to that for CAP and PC. The limiting value of O' at high frequencies is 0.025, which is close to that for CAP and about 1/4 of that for PC. Optical anisotropy of CAP and CAB will be discussed more in detail later. The C_R value for CAB was determined as the limiting O'/E' value at low frequencies ($\omega/\mathrm{s}^{-1} < 30$), where the effective contribution of the glassy component is not observed. The C_G value for CAB was determined as the limiting O''/E'' value at high frequencies. The obtained values are summarized in Table IV-2.

IV-3-2. The Rouse Segment Size of CAB and CAP

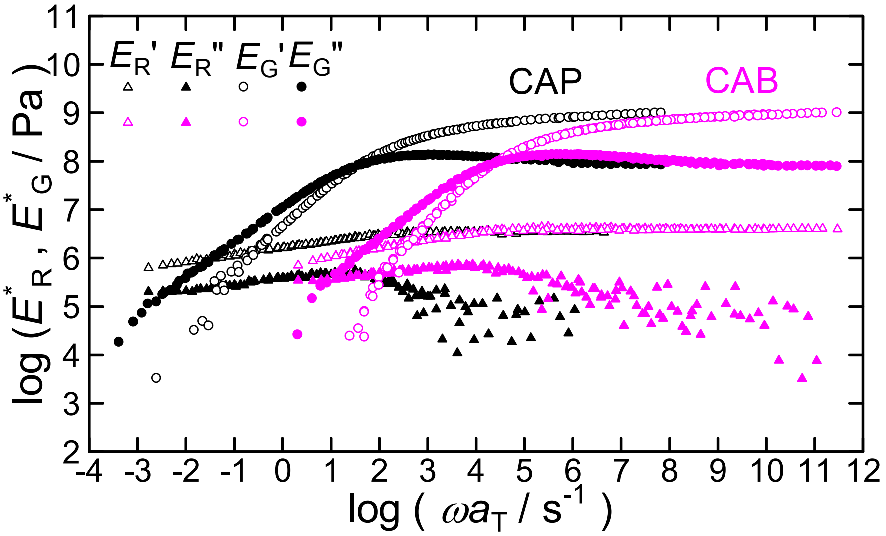

Figure IV-2. Component functions of CAB and CAP. Reference temperature is 150°C.

With the determined C_R and C_G values, the component functions, R and G, were determined by solving the MOSR, eqs. I-3 and I-4, at each temperature. The method of reduced variables was then used to obtain the composite curve for each component separately to allow the different temperature dependence between the components. Figure IV-2 shows the composite curves of the R and the G component for CAB and CAP. The G component locates at high frequencies and supports the high glassy modulus for both CAB and CAP. The frequency dependence of $E_G*(\omega)$ is somehow broader if compared with that for other amorphous polymers.[19)] This may come from the fact that friction coefficients of each repeating unit might be different because degree of substation is not uniform for each glucose unit. One may think that the broad G component may be related to the existence of the third component. However, successful and reasonable separation with two components MSOR denies such a possibility.

The R component reflects the reorientation process of the viscoelastic segments as explained earlier. From the limiting modulus at high frequencies, $E_R'(\infty)/\mathrm{Pa} = 4 \times 10^6$, for CAB is slightly larger than $E_R'(\infty)$ value for CAP (3.4×10^6/ Pa), I estimated the molar mass of the Rouse segment of CAB as 3200 g mol^{-1} with $\rho = 1200$ kgm^{-3}. This value is slightly smaller than that for CAP, 3800 g mol^{-1}, which is the *largest* among amorphous polymers to the best of our knowledge.[19)] As described before, the rubbery plateau modulus of CAB is estimated as $3G_N/\mathrm{Pa} = 7.9 \times 10^5$, and therefore number of viscoelastic segments per entanglement strand, n_e, is estimated to be 5, which is close to that for CAP.

Table IV-2. Characteristic parameters for cellulose derivative.

Polymer	E_R / MPa	E_G / GPa	$3M_N$ / MPa	M_s / g mol^{-1}	M_e / g mol^{-1}
CAP	3.4	1.1	0.78	3800	16500
CAB	4	0.9	0.79	3200	16000

IV-3-3. The Rouse Segment Size of Hypothetical Neat Cellulose

Now, I try to estimate the segment size of neat hypothetical cellulose melt by assuming that number of repeating units per Rouse segment would remain constant for hypothetical cellulose melt. In other words, I assume that esterification does not affect main chain stiffness. I estimate M_s/M_0 for CAB is 10, where M_0 is molecular weight of repeating unit. This value corresponds to that the Rouse segment is composed of 10 D-glucose units. Thus M_s for neat cellulose is estimated to be 1600 g mol^{-1}. The same analysis for CAP resulted in 1800 g mol^{-1}. Thus, I emphasis that CAP and CAB data give the consistent the Rouse segment size for the hypothetical melt of cellulose ~ 1700 g mol^{-1} irrespective of ester group.

IV-3-4. Kuhn Segment Size and Entanglement Size of Cellulose and Its Derivatives.

As described before, persistence length of cellulose depends on solvent. Among various solvent, the smallest value of q = 4.2nm, is reported for cadoxen solution.[20)] Taking this value, the molar mass of the Kuhn segment size, M_K was estimated as 2700 g mol^{-1}. This value is about 1.6 times larger than the Rouse segment size obtained in Chapter III. For many synthetic polymers, the relationship M_s~M_K holds valid in melts. Thus, M_s~M_K was not satisfied but I may conclude that my estimation of M_s for cellulose melt is consistent with the segment size of cellulose chain in solution.

Several attempts have been made to connect $M_{e,}^{melt}$ with the chain dimension. Fetters et al. proposed that G_N is proportional to cubic of the packing length, p, as mentioned in earlier.[7,8)] Hereafter, I call their approach as PL method. For calculation of p, the data on chain dimension (Kuhn segment size) is requited, which is not available for CAP and CAB. Here, I assume M_K~M_s, which widely holds well for synthetic polymers in melts. p of CAB is calculated to be 0.73 nm and M_e = 2300 $gmol^{-1}$ was obtained, being smaller that of the experimental value. Similar results were obtained for CAP.

The length, p, of neat cellulose is calculated to be 0.041 nm with q = 4.2nm for cadoxen solution. This value is about 10 times smaller than that for polystyrene. For this reason, calculated G_N^{melt} value for cellulose becomes about 1000 times larger than that for PS resulting in unrealistic entanglement size (M_e~ 10 $gmol^{-1}$). Alternatively, p and M_e can be calculated from our M_s value by setting M_K =M_s. This approach provided p =0.063nm and M_e^{melt}=90 $gmol^{-1}$. Thus, I conclude that the PL method does not work for cellulose and its derivatives, similar to linear D-glucans as discussed by Horinaka.[5)]

IV-3-5. Optical Property

Orientational birefringence, Δn, can be related to the intrinsic birefringence, Δn_0.

$$\Delta n = \Delta n_0 f \tag{IV-3}$$

Here, f is the orientation function. For tensile deformation, f is defined as

$$f = \frac{3\left\langle \cos^2\theta \right\rangle - 1}{2} \tag{IV-4}$$

Here, θ is the orientation angle which is defined as the angle between the tensile direction and the hypothetical main chain axis of the repeating units. The intrinsic birefringence can be related with the optical anisotropy of repeating units, $\Delta\alpha$.

$$\Delta n_0 = \frac{2}{9}\pi \frac{\left(\bar{n}^2 + 2\right)^2}{\bar{n}} \frac{\rho N_a}{M_0} \Delta\alpha \tag{IV-5}$$

Here, $\bar{n}$, N_a, M_0 are the mean refractive index, the Avogadro constant, and molecular weight of repeating units, respectively. For the pseudo-affine orientation$^{21)}$ f can be related to the tensile strain, ε.

$$f = \frac{3}{5}\varepsilon \tag{3}$$

Thus, the orientation birefringence in the glassy zone due to the tensile strain, $C_R E_R'(\infty)\varepsilon$ can be related to the intrinsic birefringence

$$\Delta n_0 = \frac{5}{3} C_R E_R{}'(\infty) \tag{IV-7}$$

The estimated value of Δn_0 for CAB with eq. IV-7 is 0.015. Since Δn_0 of a regenerated cellulose is reported as 0.055 [22)], $\Delta\alpha$ for CAB units are calculated to be approximately about 0.65 of that for cellulose. Estimated optical anisotropy of the polymers, $\Delta\alpha$, from the intrinsic birefringence is summarized in Table IV-3. The difference comes from the negative contribution of ester groups to anisotropy. If the chain stiffness of cellulose is not changed in solution, the C_R value for cellulose is expected as approximately 3.6×10^{-9} Pa^{-1} at 160°C and 5.7×10^{-9} Pa^{-1} at –25°C with theoretical prediction of temperature dependence of $C_R \sim 1/T$. In this context, I note that the very preliminary rheo-optical measurements indicates that C_R value for cellulose in ionic liquid is about 1×10^{-8}Pa^{-1} at –25°C. This value is about twice of C_R value for cellulose solution estimated in the previous section. The C_R value reflects the optical anisotropy of segment, $\Delta\beta$, which is determined by optical anisotropy of repeating units, $\Delta\alpha$, and number of repeating units per segments, n_S; $\Delta\beta \sim \Delta\alpha\, n_S$. Since $\Delta\alpha$ value for CAP or CAB is about half of that for cellulose as estimated in this study, the larger C_R value suggests that cellulose in ionic liquids would have a larger segment size (~3500 g mol^{-1}) than cellulose in hypothetical molten state (~1600 g mol^{-1}).

Table IV-3. Optical parameters for cellulose derivative and cellulose.

Polymer	C_R / 10^{-9} Pa^{-1}	C_G / 10^{-11} Pa^{-1}	Δn_0	$\Delta\alpha$ / 10^{-25} cm^3
CAP	2.5	1.1	0.14	6.2
CAB	2.2	1.5	0.15	6.9
Cellulose	N/A	N/A	0.055	1.1

N/A; not applicable

IV-4. Conclusions

I have determined the Rouse segment size of CAB and CAP, two cellulose esters. The molar mass of the Rouse segment of CAB in melt was 3200 g mol^{-1}, which is consistent with the value for CAP. The large M_s value reflects the rigid main chain nature of cellulose. These M_s values mean that each Rouse segment is composed of 10 glucose residues, and that the Rouse segment size M_s of cellulose in hypothetical melt is ca. 1600 g mol^{-1}. The consistent results for the two kinds of cellulose derivatives strongly suggest that this estimation is free from the effect of esterification and reflects the stiffness of linear β(1→4) linked D-glucose units faithfully. This Rouse segment size of cellulose is close to M_s of cellulose in BmimCl (= 2300 g mol^{-1}) but slightly smaller than that in EmimMP (= 4700 g mol^{-1}). Therefore, it can be concluded that M_s of cellulose is essentially concentration independent, in a sharp contrast with polystyrene.

By assuming that the ester group works as a plasticizer for cellulose, M_e/M_s for cellulose in hypothetical melts was estimated to be approximately 2, indicating a considerably small and dense entangled structure in hypothetical cellulose melt. It is noted that similar small M_e/M_s values are reported for some engineering plastics[9)] including Bisphenol-A polycarbonate[10)].

References

1) Tamai, N.; Tatsumi, D.; Matsumoto, T. *Biomacromolecules* **2004**, 5, 422.

2) Matsumoto, T.; D. T. Tamai, N.; Takaki, T. *Cellulose* **2001**, 8, 275.

3) Blachot, J. F.; Brunet, N.; Navard, P.; Cavaille, J. Y. *Rheol. Acta* **1998**, 37, 107.

4) Inoue, T.; Yamashita, Y.; Osaki, K. *Macromolecules* **2002**, 35, 9169.

5) Horinaka, J.; Okuda, A.; Yasuda, R.; Takigawa, T. *Colloid. Polym. Sci.* **2012**, 290, 1793.

6) Yamaguchi, M.; Lee, S.; Manaf, M. E. A.; Tsuji, M. *Eur. Polym. J.* **2010**, 46, 2269.

7) Fetters, L. J.; Lohse, D. J.; Graessley, W. W. *J. Polym. Sci. Part B: Polym. Phys.* **1999**, 37, 1023.

8) Fetters, L. J.; Lohse, D. J.; Milner, S. T.; Graessley, W. W. *Macromolecules* **1999**, 32, 6847.

9) Hwang, E. J.; Inoue, T.; Osaki, K. *Polym. Eng. Sci.* **1994**, 34, 135.

10) Inoue, T.; Hwang, E. J.; Osaki, K. *J. Rheol.* **1992**, 36, 1737.

11) Yamaguchi, M.; Okada, K.; Edeerozey, M.; Shiroyama, Y.; Iwasaki, T.; Okamoto, K. *Macromolecules* **2009**, 42, 9034.

12) Yamaguchi, M.; Iwasaki, T.; Okada, K.; Okamoto, K. *Acta Mater.* **2009**, 57, 823.

13) Hutcheson, S. A.; McKenna, G. B. *J. Chem. Phys.* **2008**, 129, 074502.

14) Schroter, K.; Hutcheson, S. A.; Shi, X.; Mandanici, A.; McKenna, G. B. *J. Chem. Phys.* **2006**, 125, 214507.

15) Ferry, J. D. *Viscoelastic Properties of Polymers* Wiley: New York, **1980**, p. 672.

16) Inoue, T.; Hayashihara, H.; Okamoto, H.; Osaki, K. *J. Polym. Sci. Polym. Phys. Ed.* **1992**, 30, 409.

17) Inoue, T.; Okamoto, H.; Osaki, K. *Macromolecules* **1991**, 24, 5670.

18) Osaki, K.; Inoue, T.; Uematsu, T.; Yamashita, Y. *J. Polym. Sci. B Polymer Physics* **2001**, 39, 1704.

19) Inoue, T.; Osaki, K. *Macromolecules* **1996**, 29, 1595.

20) McCormick, C. L.; Callais, P. A.; Hutchinson, B. H. *Macromolecules* **1985**, 18, 2394.

21) Inoue, T. *Macromolecules* **2006**, 39, 4615.

22) Hermans, P. H. *Physics and Chemistry of Cellulose Fibres,* Elsevier: New York, **1949***,* p. 556.

Chapter V. Comparison between Cellulose and Other Polysaccharides.

V-1. Introduction

Ionic liquids have been utilized as solvents for several polysaccharides as well as for cellulose. Recently, Horinaka *et al.* have reported viscoelastic properties of polysaccharides in ionic liquids and have discussed the entanglement features of polysaccharides such as cellulose, amylose, pullulan, and curdlan, in BmimCl.[1-5] Amylose is an α-glucans with α(1→4) bond and pullulan is an α-glucans with the sequence of α(1→4), α(1→4), and α(1→6) bonds. Curdlan is β-glucan consisting of β(1→3) linked glucose units. The chemical structures of these polysaccharides are showed in Figure V-1. Horinaka *et al.* determined the molar mass between entanglement points in molten state, $M_{\mathrm{e,melt}}$, for the above polysaccharides. According to their result, the value of $M_{\mathrm{e,melt}}$ varied with type of polysaccharides, suggesting that the linkage between glucose units affect the entanglement structure. Assuming that $M_{\mathrm{e,melt}}$ reflects the chain rigidity[6], the linkage type should affect the chain rigidity. In fact, Horinaka *et al.* argued that $M_{\mathrm{e,melt}}$ is a decreasing function of the characteristic ratio reflecting the chain rigidity. However, the relationship between the chain rigidity and the linkage type has not been clarified yet.

As mentioned in Chapter I, the origin of the cellulose chain rigidity is suggested due to β-linkage. Thus, it is significant to discuss the relationship between the cause of the chain rigidity and the linkage type. In particular, the conformational difference could be largely appeared in α-glucans and β-glucans. The helical structure, typically suggesting for amylose, should also affect the chain rigidity.

In this study, dynamic viscoelasticity and birefringence were measured for two typical α-glucans, amylose and pullulan, in BmimCl from dilute to concentrated state to estimate their

Rouse segment sizes. Moreover, the concentration dependences of the Rouse segment size were compared with that of cellulose in order to discuss the relationship between the chain rigidity and linkage type.

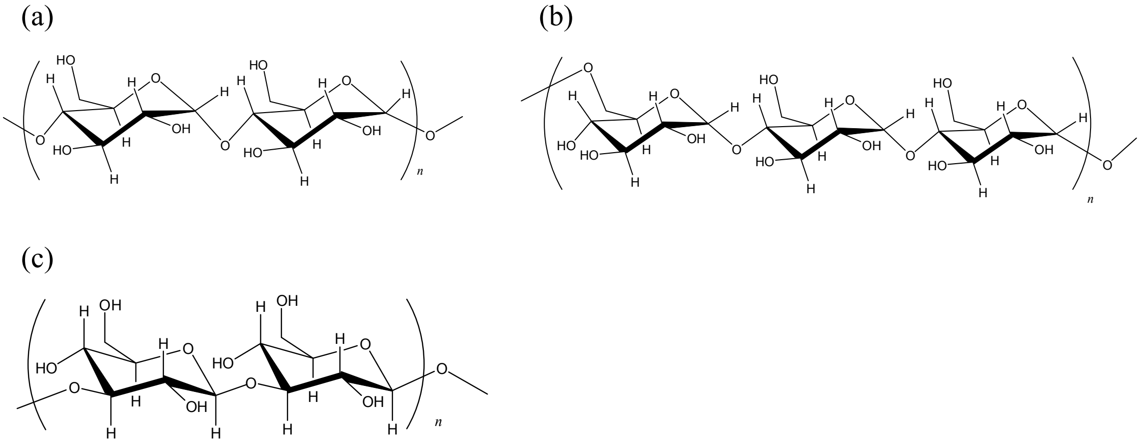

Figure V-1. Chemical structure of amylose (a), pullulan (b), and curdlan (c).

V-2. Experimental

Materials and Preparation of Solutions. The amylose sample was purchased from Wako Pure Chemical Industries, Ltd (*M* ~ ca. 15,000). The pullulan sample was kindly supplied by Prof. T. Shikata (Tokyo University of Agriculture and Technology). 1-butyl-3-methylimidazolium Chloride (BmimCl) purchased from Wako Pure Chemical Industries, Ltd was used without further purification. The polysaccharides and BmimCl were dried in a vacuum oven overnight. The dried polysaccharides were dissolved into liquid BmimCl in a vacuum oven at 100˚C for 48 hours. Concentration of the polysaccharid ranges from 3 to 40 wt% for amylose and 3 to 30 wt% for pullulan.

Measurements. The viscoelastic measurements and the simultaneous measurements of stress and flow birefringence were carried out in the same manner as the cellulose / BmimCl solution (cf. Chapter III).

V-3. Results and Discussion

V-3-1. Estimation of the Polymer Contribution

Dilute Region. The complex modulus, G^*, and strain-optical coefficient, K^*, for amylose and pullulan at dilute concentration (3%) were shown in Figure V-2 (a) and (b). The spectra were similar to those of the cellulose solution (2%). I used the same shift factor to construct master curves for G^* and K^*. As in the case of cellulose, a systematic deviation was observed in K'' for both amylose and pullulan in the range of $-1 < \log (\omega a_T / \mathrm{s}^{-1}) < 1$. The characteristic relationship, $G' \propto \omega^2$ and $G'' \propto \omega^1$, in the terminal flow zone appears only at $\log (\omega a_T / \mathrm{s}^{-1}) < 2$. In the glassy zone, G^* is almost identical to that of pure BmimCl, and the polymer contribution to G^* becomes significant at lower frequencies. Since the polymer contribution to K' is more significant than that to G', the composite curve for K' has a plateau in the intermediate frequency region, which enables us to estimate the Rouse segment size from K' more accurately. K_{RZ}'' was calculated using $K'' - \omega C_S(T) \eta_S(\infty) a_T$ with the same manner as the cellulose dilute solution (Chapter III). The stress–optical coefficients for polymer component, C_{RZ}, were obtained as 2.2×10^{-9} Pa^{-1} for amylose and 2.7×10^{-9} Pa^{-1} for pullulan.

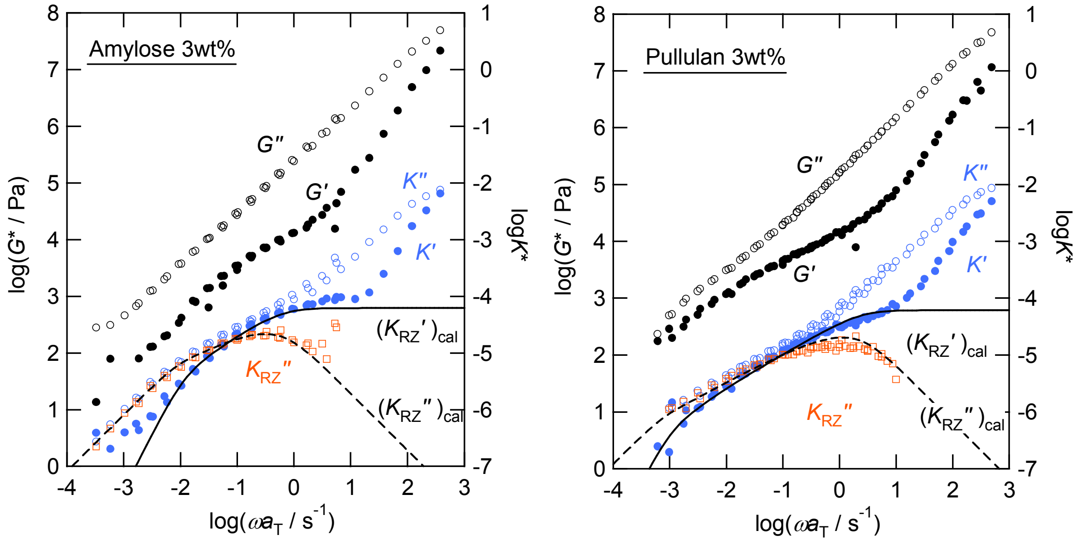

Figure V-2. Frequency dependence of G^* and K^* for amylose and pullulan solutions at 3 wt%. Reference temperature, T_r, is −25 °C. $K_\mathrm{RZ}{}^*$ was calculated with $K_\mathrm{RZ}{}^* = K^* - \mathrm{i}S_\mathrm{S}(\infty, T)\omega$. Lines represent Rouse−Zimm theoretical curve.

Concentrated Region. Figure V-3 and 4 show the master composite curves of G^* and K^* for amylose and pullulan at higher concentrations. The solvent dynamics is significantly modified by the presence of polymer chain at higher concentration. Therefore, the polymer contribution is obtained by subtracting the modified solvent contribution. For cellulose solution, the modified stress–optical rule (MSOR) was successful for the estimation of polymer contribution (Chapter III). For also amylose and pullulan solutions, the polymer component, $G_\mathrm{RZ}{}^*$, and the glassy component, $G_\mathrm{G}{}^*$, were estimated by MSOR (Figure V-5 and 6). The stress–optical coefficients of each component, C_RZ and C_G were experimentally determined. $G_\mathrm{RZ}{}'$ at all concentrations has a plateau in the high frequency region, which enables us to estimate the Rouse segment size, as described later. It should be noted that $G_\mathrm{G}{}^*$ at all concentrations shows the broader relaxation than that of neat BmimCl. This means that the glassy component could not be explained by just the dynamics of neat solvent.

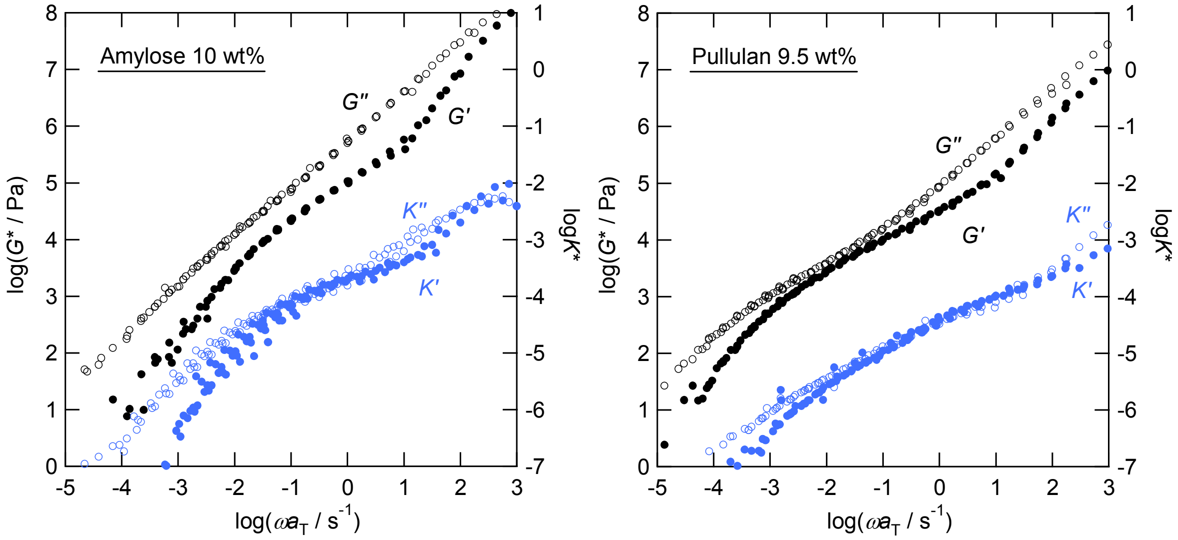

Figure V-3. Frequency dependence of G^* and K^* for amylose and pullulan solutions at 10 and 9.5 wt% respectively. Reference temperature, T_r, is −25 °C.

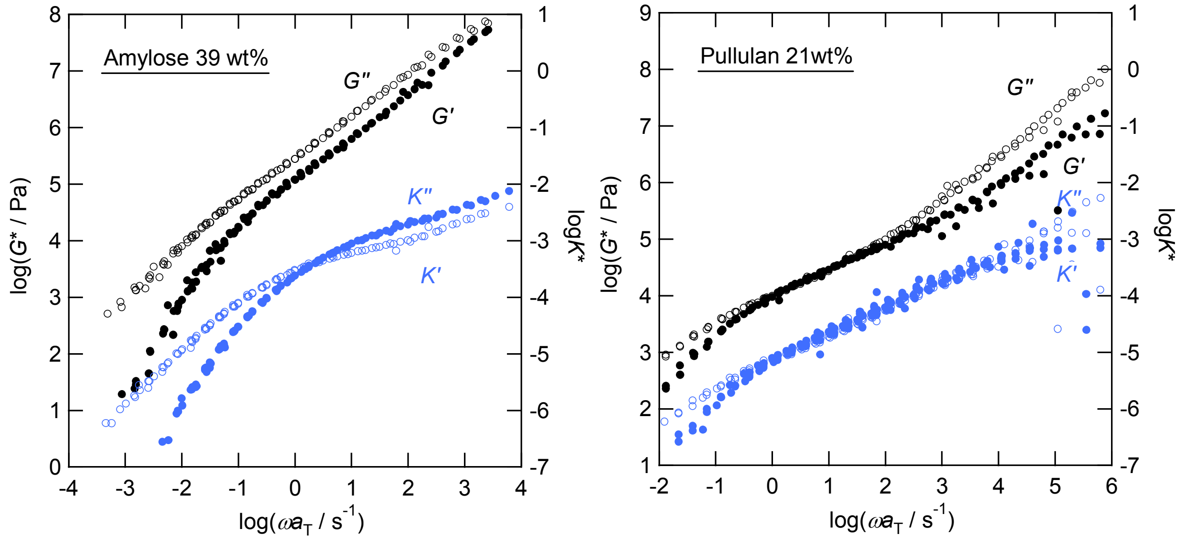

Figure V-4. Frequency dependence of G^* and K^* for amylose and pullulan solutions at 39 and 21 wt% respectively. Reference temperature, T_r, is 25 °C.

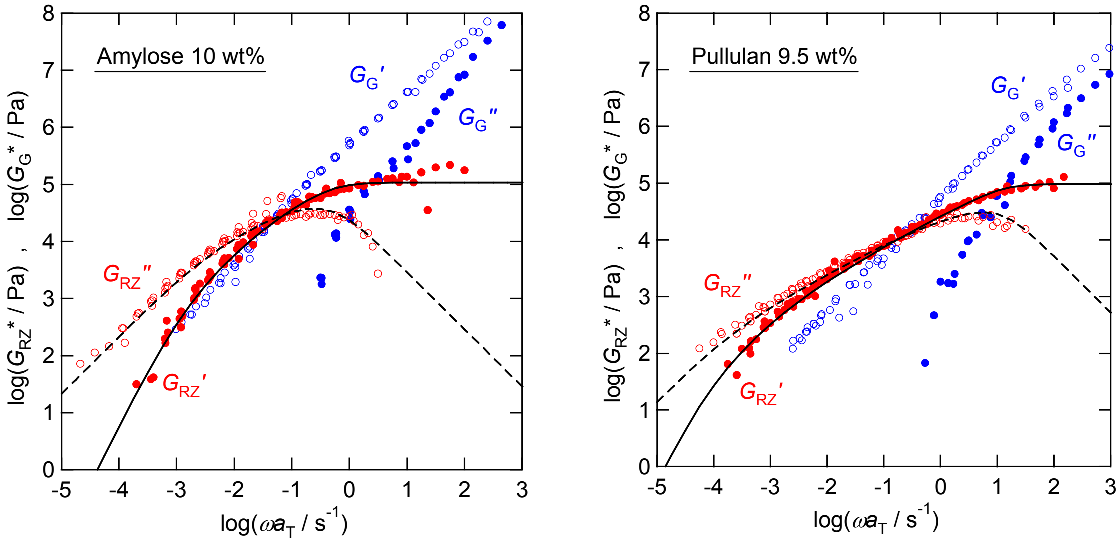

Figure V-5. Rouse−Zimm and glassy contributions of G* for amylose and pullulan solutions at 10 and 9.5 wt% respectively. Reference temperature, T_r, is −25 °C. Lines represent Rouse−Zimm theoretical curve for G_{RZ}*.

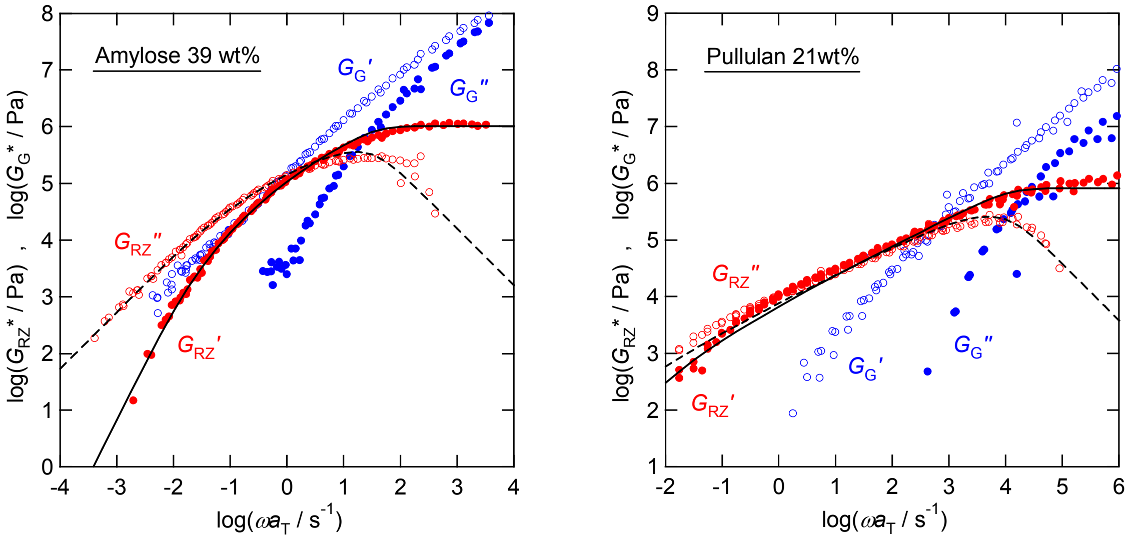

Figure V-6. Rouse−Zimm and glassy contributions of G* for amylose and pullulan solutions at 39 and 21 wt% respectively. Reference temperature, T_r, is 25 °C. Lines represent the Rouse−Zimm theoretical curve for G_{RZ}*.

V-3-2. Estimation of the Rouse Segment Size

The Rosue–Zimm theory was applied for determination of the Rouse segment size of amylose and pullulan in solution as well as cellulose in solution (Chapter III). According to the theory, the polymer contribution of the linear polymer solution with polymer mass concentration, c, is given by

$$\left(G_{RZ}^{*}(\omega)\right)_{cal} = \sum_{M=0}^{\infty} x_M \frac{cRT}{M} \sum_{i=1}^{N} \frac{i\omega\tau_P}{1+i\omega\tau_P} \tag{V-1}$$

$$\left(K_{RZ}^{*}(\omega)\right)_{cal} = C_{RZ} \sum_{M=0}^{\infty} x_M \frac{cRT}{M} \sum_{i=1}^{N} \frac{i\omega\tau_P}{1+i\omega\tau_P} \tag{V-2}$$

$$\tau_P = \frac{\tau_{RZ}}{p^k} \quad (1.5 \le k \le 2) \tag{V-3}$$

Here, RT is the gas constant multiplied by the absolute temperature, M and N are the molecular weight and number of segments per chain of the polymer, respectively, and τ_{RZ} is the longest relaxation time of the bead-spring model. For natural polymers, molecular weight distribution should be considered. x_{M} is the number fraction of polymers with the molecular weight, M. For the case of most probable distribution, x_{M} is represented by eq V-4.

$$x_{\mathrm{M}} = \frac{1}{M_{\mathrm{n}}} \exp\left(-\frac{M}{M_{\mathrm{n}}}\right) = \frac{2}{M_{\mathrm{w}}} \exp\left(-\frac{2M}{M_{\mathrm{w}}}\right) \tag{V-4}$$

Black solid and dashed curves for G' and G'', respectively, in Figures V-1, V-4, and V-5 indicate theoretical values calculated by eqs V-1–V-4. I have chosen the number averaged molecular mass, $M_{\mathrm{n}}^{\mathrm{app}}$, of amylose and pullulan to be 10,000 (3%) and 150,000 (3%), respectively, to obtain a good fitting of the low frequency region data with k=2 corresponding to the Rouse model. This exponent may be natural because the concentration is close to c^* and therefore the hydrodynamic interactions would be screened out. It should be note that the above analysis at a finite concentration gives an apparent molecular weight, $M_\mathrm{n}^\mathrm{app}$, due to the effect of inter-chain interaction (refer in detail in Chapter III). The value of $M_\mathrm{n}^\mathrm{app}$ used for theoretical curve in the Figures was summarized in Table V-1. For amylose solutions, $M_\mathrm{n}^\mathrm{app}$ was constant at all concentration. This indicates that

$M_\mathrm{n}^\mathrm{app}$ corresponds to $M_\mathrm{n}^\mathrm{true}$, because c^* is higher enough than c. On the other hand, for pullulan solutions, the higher concentration is, the larger value of $M_\mathrm{n}^\mathrm{app}$ is. This means c^* is lower than c at least 10%, because $M_\mathrm{n}^\mathrm{true}$ is large enough. Theoretical curve could not describe experimental results, because the effect of inter-chain interaction is too large in $c > 21\%$.

Table V-1. The value of apparent molecular weight, $M_\mathrm{n}^\mathrm{app}$, selected for theoretical curve

c / wt%	Amylose	Pullulan
3.0	1.0×10^4	2.0×10^5
10	1.0×10^4	3.0×10^5
21		$> 8.5\times10^5$
28		$> 8.5\times10^5$
39	1.0×10^4	

The Rouse segment size can be automatically estimated by fitting the data of G_RZ^*. The limiting modulus at high frequencies, $G'_\mathrm{RZ}(\infty)$, can be obtained more easily and precisely.

The Rouse segment size, M_s, was estimated by

$$M_\mathrm{S} = \frac{cRT}{G_\mathrm{RZ}'(\infty)} \tag{V-5}$$

Using SOR, the Rouse-Zimm theory can be also applied to $K_{\mathrm{RZ}}*$, which is calculated by $C_{\mathrm{RZ}}G_{\mathrm{RZ}}*$. M_{s} was estimated by eq V-6 for dilute solutions.

$$M_{\mathrm{S}} = \frac{C_{\mathrm{RZ}} cRT}{K_{\mathrm{RZ}}'(\infty)} \tag{V-6}$$

The obtained value of M_{s} for amylose and pullulan at all concentrations was summarized in Tabel V-2.

Table V-2. The Rouse segment size, M_{s} / g mol^{-1}, obtained by fitting the data of $G_{\mathrm{RZ}}*$

c / wt%	Amylose	Pullulan
3.0	2.2×10^3	2.7×10^3
10	1.5×10^3	2.1×10^3
21		6.0×10^3
28		5.0×10^3
39	9.0×10^2	

V-3-3. Concentration Dependence of the Rouse Segment Size

Concentration dependence of the molar mass of the Rouse segment, M_{s}, for amylose and pullulan (listed in Table V-2) along with that for cellulose (chapter III) is shown in Figure V-7. The value of M_{s} for cellulose at high concentrations is lacking in the data due to poor solubility of cellulose. Therefore, the value of $M_{\mathrm{s}} \sim 1700$ g mol^{-1} for hypothetical cellulose melt estimated by cellulose derivatives (see chapter IV) was used as a reference of concentrated cellulose solution. While M_{s} of cellulose essentially shows no concentration dependence, those for amylose and pullulan clearly depend on the concentration like polystyrene. For polystyrene, a typical flexible polymer, it is known that M_s at dilute regime is more than 5 times larger than that in the concentrated region7). The concentration dependence of M_s suggests that relative rigidity of the polymer chain surrounded by solvent molecules increases with decreasing concentration. In other words, the change of M_s is due to the interaction between polymer and solvent. At the lowest concentration, M_s values for these three polysaccharides are almost identical. This suggests that dynamical rigidity is independent of polymer spices, because the dynamical rigidity at dilute solution is mainly affected by solvent molecules. The present experimental result of concentration dependence shows the extent of changing the dynamical chain rigidity depends on polymer species. Weak concentration dependence of cellulose reflects the symmetric structure between repeating unit due to β(1→4) linkage. On the other hand, amylose and pullulan showed concentration dependence, suggesting more flexibility of chain as α−glucans. While M_s had only 30 % deviation among three polysaccharides at 0.1 g cm^{-3}, M_s of pullulan was over 3 times small as cellulose at higher concentration. In the higher concentration region, molecular interactions could be screened out in the scale of the Rouse segment. The own Rouse segment size should be appeared in this region. Judging from the value of M_s at the highest concentration, pullulan shows the smallest value, indicating the chain flexibility. This result is consistent with the small persistence length obtained light scattering measurement for pullulan in an ionic liquid. (see Chapter II-3-4)

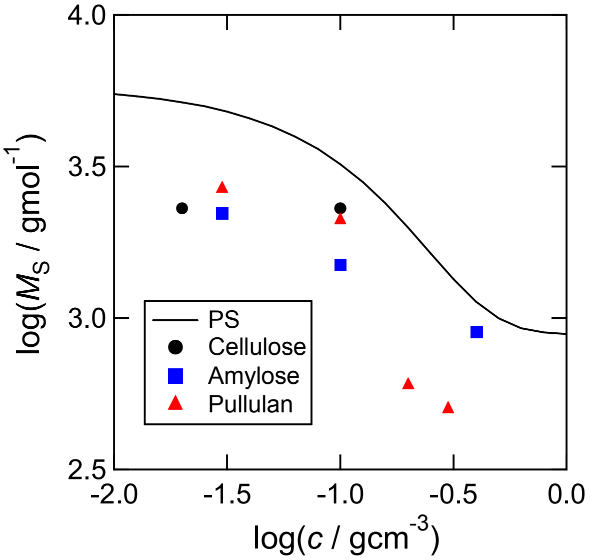

Figure V-7. Concentration dependence of the molar mass of the Rouse segment for amylose, pullulan, and cellulose, as well as polystyrene.

V-3-4. Concentration Dependence of the Stress-Optical Coefficient

The concentration dependence of the stress-optical coefficient of the Rouse-Zimm component, C_{RZ}, for cellulose, amylose, and pullulan is showed in Figure V-7. The coefficient C_{RZ} is dependent not only on the size of the Kuhn segment but also on anisotropy of the repeating unit, and therefore, one needs additional information about the polymer chain to discuss C_{RZ}. For cellulose, C_{RZ} is almost independent on the polymer concentration, while C_{RZ} for pullulan strongly depends on the polymer concentration, both in accordance with the concentration dependence of M_{s}. On the other hand, amylose essentially shows no concentration dependence of C_{RZ}, in contrast with the concentration dependence of M_{s}. This concentration independence of C_{RZ} for amylose may come from a cancelation of the concentration dependences of M_{s} and the optical segment size. The value of C_{RZ} of cellulose is 10 times larger than those of amylose and pullulan, suggesting the highest anisotropy of the cellulose chain.

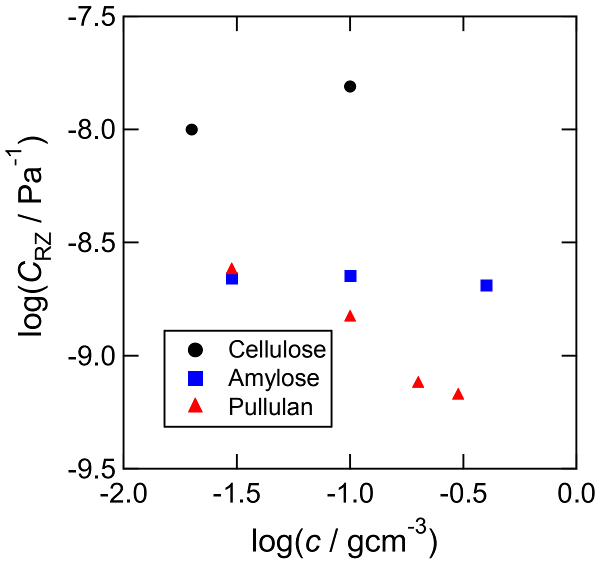

Figure V-8. Concentration dependence of the stress−optical coefficients of the Rouse−Zimm component for amylose, pullulan, and cellulose in BmimCl.

V-4. Conclusions

Simultaneous measurements of viscoelasticity and birefringence were carried out for BmimCl solutions of amylose and pullulan at various temperatures covering a wide frequency zone. The spectra of G^* and K^* were similar to the cellulose solution. For dilute solutions, the polymer contribution was obtained by subtracting the solvent contribution. For concentrated solutions, the polymer contribution was obtained by MSOR. The Rouse segment size, M_s, was estimated by the Rouse-Zimm theory.

The Rouse segment size at high concentrations was larger in order of cellulose > amylose > pullulan. This result was consistent with the Kuhn segment length. At the lowest concentration, M_s values for these three polysaccharides are almost identical. This agreement may occur by accident, because b_K, b, and ΔE_a appearing in eq III-22 in Chapter III are all different among the three polysaccharides. Experimental result of concentration dependence shows the extent of changing the dynamical chain rigidity depends on polymer species. According to Larson's theory (Chapter III), concentration dependence of M_s was determined by the value of ΔE_a. Weak concentration dependence of cellulose reflects the symmetric structure between repeating unit due to β(1→4) linkage. The stress-optical coefficient of polymer component, C_{RZ}, has same tendency as concentration dependence of M_s.

References

1) Horinaka, J.; Okuda, A.; Yasuda, R.; Takigawa, T. *Colloid Polym. Sci.* **2012,** 17, 1793.

2) Horinaka, J.; Yasuda, R.; Takigawa, T. *J. Polym. Sci. Part B: Polym. Phys.* **2011,** 49, 961.

3) Horinaka, J.; Yasuda, R.; Takigawa, T. *Polym. J.* **2011,** 43, 1000.

4) Horinaka, J.; Honda, S.; Takigawa, T. *Carbohydr. Polym.* **2009,** 78, 576.

5) Horinaka, J.; Yasuda, R.; Takigawa, T. *J.Appl. Polym.Sci.* **2012,** 123, 3023.

6) Graessley, WW.; Edwards SF. *Polymer* **1981,** 22, 1329.

7) Inoue, T.; Uematsu, T.; Osaki, K. *Macromolecules* **2002,** 35, 820.

Chapter VI. Summary

This thesis focuses on the static and dynamic chain rigidities of the cellulose chain in ionic liquid solutions. Light scattering measurements were performed for cellulose/ionic liquid solutions to discuss the static chain rigidity. On the other hand, simultaneous measurements of viscoelasticity and flow birefringence were carried out to determine the dynamic chain rigidity. The comparison of the static and dynamic chain rigidities made it possible to understand the interrelation between the conformation and dynamics of the cellulose chain in ionic liquids comprehensively. In addition, the effect of the polymer chain stiffness on the relation between the conformation and dynamics of the polymer chain was examined by comparing the relation for cellulose with those for some other polysaccharides with the different glycosidic linkage type as well as for polystyrene, a flexible polymer.

In Chapter II, the conformational study was carried out for cellulose in ionic liquid solutions by light scattering measurements. Two ionic liquids, EmimMP and EmimDMP were used for solvents of the light scattering study. The molecular weight dependence of the hydrodynamic radius for cellulose in the two ionic liquids obtained was analyzed in terms of the wormlike cylinder model. From the analysis, the persistence length of cellulose in EmimMP and EmimDMP was determined to be 7 nm, which is comparable to those for cellulose in other solvents, but much larger than that for pullulan in EmimDMP. Thus, it was concluded that cellulose behave as a semiflexible polymer in ionic liquids.

Chapter III reports the rheo-optical data for BmimCl and EmimMP solutions of cellulose. The data were analyzed to estimate the molar mass of the Rouse segment M_s of cellulose in the two ionic liquids. The result of M_s in EmimMP was almost same as the molar mass of the Kuhn segment M_K for cellulose in the same solvent which was obtained from the persistence length determined by light scattering described in Chapter II. This indicates that the static and dynamic chain rigidities are almost identical for cellulose in solution. Furthermore, M_s of cellulose in BmimCl did not depend on the cellulose concentration. These results with respect to M_s for cellulose form a remarkable contrast with M_s reported for typical flexible polymer polystyrene, where M_s is 5 times as large as M_K in solution, but reduces with increasing the polymer concentration to be equal to M_K in bulk. These results lead to the conclusion that the ration between the static and dynamic rigidities depends on the chain stiffness.

In Chapter IV, the Rouse segment sizes of cellulose esters, CAB and CAP, in bulk were estimated from rheo-optical data. The results of M_s for the two cellulose derivatives in bulk provided M_s of cellulose in hypothetical melt, which was almost identical with that of cellulose in BmimCl. This strongly indicates that the dynamic rigidity of cellulose is independent of the cellulose concentration over the entire concentration range from dilute to bulk.

In Chapter V, rheo-optical measurements were extended to more flexible polysaccharides, amylose and pullulan, in BmimCl solutions. The M_s value obtained in concentrated BmimCl solutions was higher in order of cellulose > amylose > pullulan. These results are consistent with the order of M_K of the three polysaccharides.

List of Publications:

This thesis work has been or will be published in the following papers.

1) “On the Viscoelastic Segment Size of Celluose”

   Maeda, A.; Inoue, T. *Nihon Reoroji Gakkaishi* **2011**, 39, 159.

2) “Dynamic Segment Size of the Cellulose Chain in an Ionic Liquid”

   Maeda, A.; Inoue, T.; Sato, T. *Macromolecules* **2013**, 46, 7118.

3) “Dynamic Rigidity of Cellulose Derivatives in Melts”

   Maeda, A.; Inoue, T.; Yamaguchi, M. *Polymer Journal,* doi:10.1038/pj.2013.73.

4) “Light Scattering Study on Linear D-glucans in Ionic Liquids”

   Maeda, A.; Sato, T. to be submitted.

5) “Dynamic Segment Size of Polysaccharides with Different Glucosidic Linkages in Ionic Liquids”

   Maeda, A.; Inoue, T.; Sato, T. to be submitted.